Electronic Supplementary Information

Multivariate Zeolitic Imidazolate Frameworks with an Inverting Trend in Flexibility

Arijit Halder,[a] Ryan A. Klein,[b,c] Rachel Lively,[a] and C. Michael McGuirk*[a]

[a]Department of Chemistry, Colorado School of Mines, Golden, Colorado, 80401 USA.

[b]Material, Chemical, and Computational Sciences Directorate, National Renewable Energy Laboratory, Golden, Colorado 80401, USA

[c]Center for Neutron Research, National Institute of Standards and Technology, Gaithersburg, Maryland 20899, USA

*Correspondence to: cmmcguirk@mines.edu

Table of Contents

General Procedures

General Synthesis and Characterization Methods.

All the reagents at reagent grade purity were obtained from commercial sources and were used as received except 2-methyl-5,6-difluorobenzimidazole which was synthesized following a previously published procedure.[1] Benzimidazole (98%) and 4,5-Difluorobenzene-1,2-diamine (98%) was purchased from Sigma–Aldrich.† Cadmium perchlorate hydrate was purchased from Strem Chemicals. All solvents were purchased from VWR. Ultrahigh purity (99.999%) He, N_2, and propane were used for all adsorption experiments.

Propane Adsorption Isotherms.

All the propane isotherms were measured using a Micromeritics ASAP 2020 plus instrument. In a typical measurement, 100–200 mg of powdered sample was placed in a pre-weighed glass measurement tube and capped with a Micromeritics TranSeal. All the samples were degassed on the adsorption instrument at 150 °C for 16 hours (outgas rate < 4 μbar/min). Then the evacuated tube was removed from the instrument and weighed to determine the mass of the degassed sample. Then the tube was then transferred to the analysis port of the adsorption instrument, where the outgas rate was again confirmed to fall below 2 μbar/min. Propane isotherms are collected at water bath at 25 °C, 14 °C and 4 °C, maintained by a temperature-controlled water circulator. For propane gas adsorption measurements at different temperatures, data were collected following a common strategy employed to ensure sufficient data density and resolution at and around the gate opening, as well as to ensure that the data collection ends at a physically meaningful time. First the full region was divided into few sections and a fixed increment of pressure was considered for each section. For the first section the increment was 5 mmHg pressure which was incremented up to 50 mmHg at the very end of the data collection. The equilibrium interval was 30 seconds with a maximum volume increment was set to instrument's default value which is 20 cm^3/g. Additionally, some extra points were added manually in the vicinity of the gate opening to increase data resolution during the gate opening phenomenon.

Nitrogen Adsorption Isotherms.

All the N_2 isotherms were measured using a Micromeritics ASAP 2020 plus instrument over relative pressure range 0−1. In a typical measurement, 100–200 mg of powdered sample was placed in a pre-weighed glass measurement tube and capped with a Micromeritics TranSeal. All the samples were degassed on the adsorption instrument at 150 °C for 16 hours (outgas rate < 4 μbar/min). Then the evacuated tube was removed from the instrument and weighed to determine the mass of the degassed sample. Then the tube was transferred to the analysis port of the adsorption instrument, where the outgas rate was again confirmed to fall below 2 μbar/min. Isotherms are collected in a 77 K liquid N_2 bath. For all the nitrogen gas adsorption isotherm measurements, data were collected following a common strategy employed to ensure sufficient data density and resolution at and around the gate opening, as well as to ensure that the data collection ends at a physically meaningful time. First the full region was divided into a few sections and a fixed increment of pressure was considered for each section. For the first section the relative pressure increment was 0.02 mmHg which was incremented up to 0.05 mmHg at the very end of the data collection. The equilibrium interval was set to 30 seconds with a maximum volume increment set to the instrument's default value, which is 20 cm^3/g. Additionally, some extra points manually programmed in the vicinity of the gate opening to increase data resolution during the gate opening phenomenon.

Powder X-ray Diffraction Patterns

Powder X-ray diffraction (PXRD) patterns were collected using a Bruker D2 Phaser benchtop powder X-ray diffractometer with Cu Kα radiation ($K\alpha_1$ λ = 1.54056 Å, $K\alpha_2$ λ = 1.54439 Å), and a Lynxeye XE-T linear position-sensitive detector, and the following optics: fixed divergence slit (1 mm), anti-scatter screen (1 mm), receiving slit (3 mm), and secondary-beam Soller slits (2.5°). Generator settings were 30 kV and 10 mA. All the powder X-ray diffraction patterns were collected at room temperature in air unless it is mentioned otherwise.

NMR Spectroscopy Analysis of Digested Frameworks.

Approximately 10 mg of powder sample was added to a total of 0.7 mL deuterated solvent and ^1H or ^{19}F NMR spectra were acquired on a JEOL ECA-500 NMR spectrometer. For the ligand 2-methyl-5,6-benzimidazole (2M56DFbim), trifluoroacetic acid-d_1 or DMSO–d_6 were used as the solvent for data acquisition. For all the multivariate MOFs, NMR spectra were taken after digesting in 0.7 mL of trifluoroacetic acid-d_1. For these systems the different signals are identified and assigned for the proton from either benzimidazole or 2-methyl-5,6-

benzimidazole (or solvent). Then integral values for different protons from the two different ligands are compared to evaluate the ratio of the individual ligands in the system.

Synthesis, Activation and Characterization

Synthesis of 2-methyl-5,6-difluorobenzimidazole

This procedure was adapted from that originally reported by Kriete *et al.*[1]

In a 10 mL round bottom flask, 4,5-Difluorobenzene-1,2-diamine (3 g, 20.86 mmol) and acetic acid (2.5 mL, 43.74 mmol) were heated at 120 °C under nitrogen atmosphere for 6 h. Completion of the reaction is confirmed by thin-layer chromatography (TLC). After cooling down to room temperature, 1 M NaOH was added to the reaction mixture to reach a pH just above 7. Then the reaction mixture was diluted with water (300 mL) and extracted with ethyl acetate (5 x 50 mL). Combined organic layers were dried over anhydrous $MgSO_4$, filtered, and concentrated to get pure product (3.1 g, 89%).

^{1}H NMR (500 MHz, DMSO-d_6) δ = 12.37 (s, 1H), 7.45 (t, J = 9.4 Hz, 2H), 2.43 (s, 3H).

^{1}H NMR (500 MHz, Trifluoroacetic acid-d_1) δ = 7.48 (t, J = 7.3 Hz, 2H), 2.85 (s, 3H).

^{19}F NMR (471 MHz, DMSO-d_6) δ = −146.04 (d, J = 592.8 Hz).

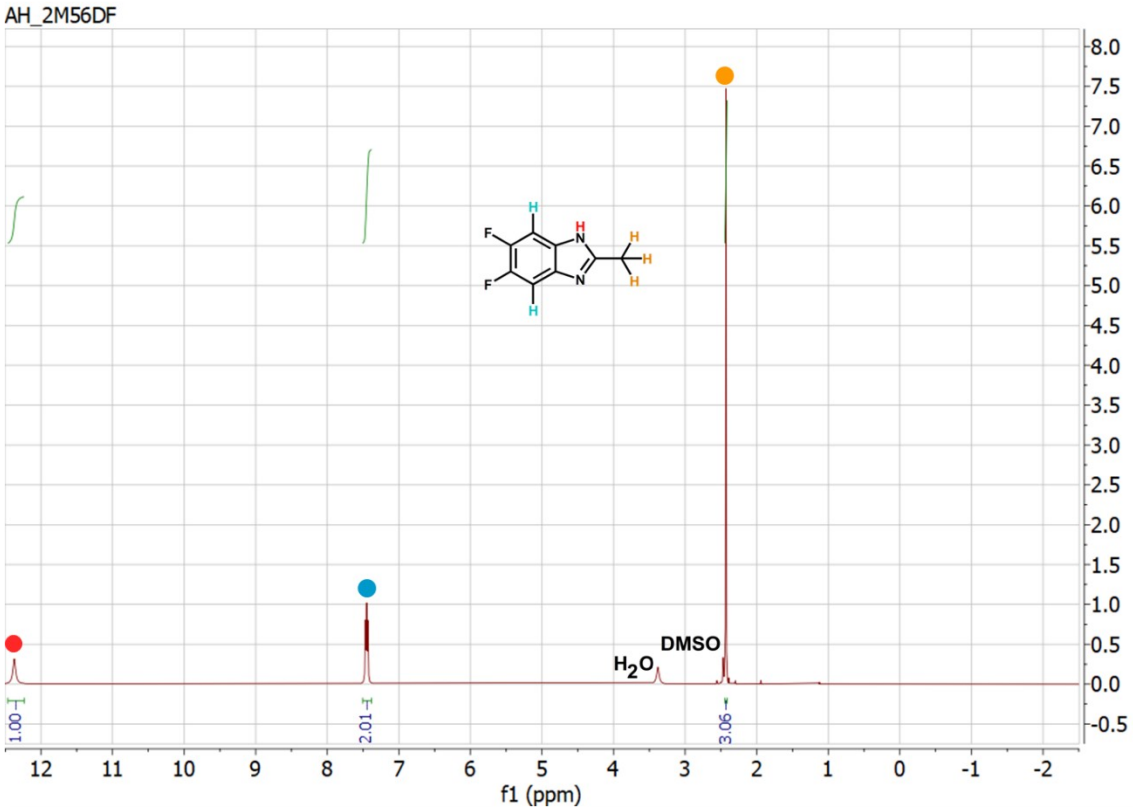

Fig. S1. ^{1}H NMR spectrum of 2-methyl-5,6-difluorobenzimidazole (~10 mg in DMSO–d_6. 500 MHz).

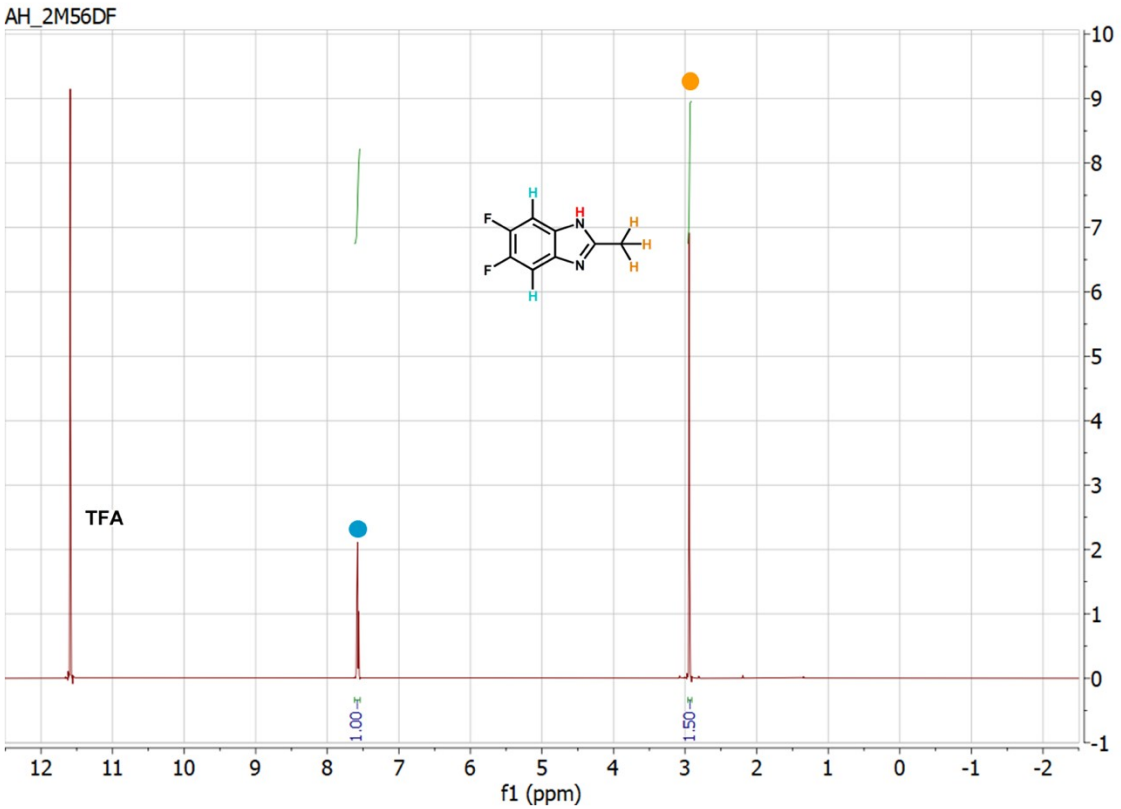

Fig. S2. [1]H NMR spectrum of 2-methyl-5,6-difluorobenzimidazole (~10 mg in Trifluoroacetic acid–d_1. 500 MHz).

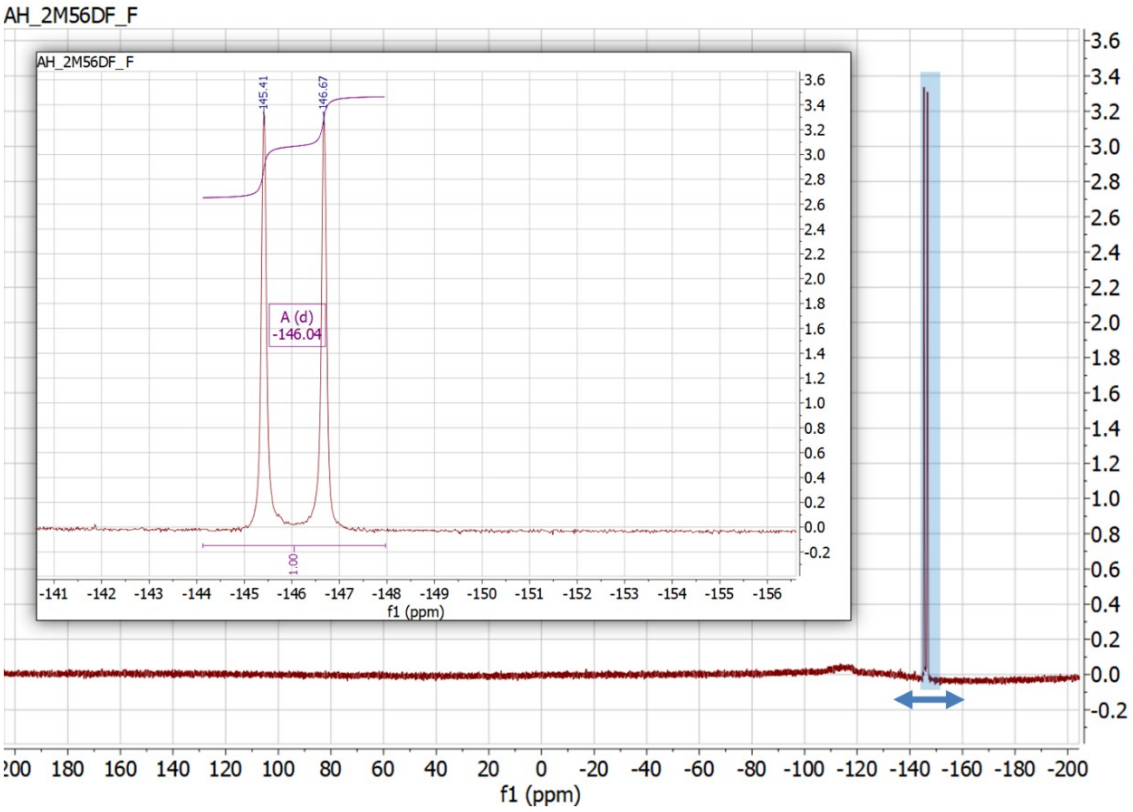

Fig. S3. [19]F NMR spectrum of 2-methyl-5,6-difluorobenzimidazole (~10 mg in DMSO–d_6. 471 MHz). Inset is the zoomed part of the marked portion of the full spectrum.

Synthesis and activation of CdIF-13

The synthetic procedure was adapted from a previously reported procedure[2] with minor changes. Please note, the cadmium salt, $Cd(ClO_4)_2 \cdot xH_2O$, used in this procedure is an oxidant and is acutely toxic. This chemical should be handled with necessary precautions.

A 4 mL scintillation vial was charged with $Cd(ClO_4)_2 \cdot xH_2O$ (300 mg), benzimidazole (118 mg, 1 mmol) and 2 mL of *N,N*-dimethylformamide (DMF). The vial was closed with a Teflon lined cap and sonicated until reaching a clear, colorless solution. This was then heated to 130 °C in an oven for 24 h. Afterwards, the vial was slowly cooled to room temperature by turning the oven off and allowing it to cool down naturally without opening the oven door. Colorless crystals of CdIF-13 were collected by vacuum filtration and washed with excess DMF to remove any unreacted starting materials. Then thoroughly washed with dichloromethane (CH_2Cl_2) to remove any excess DMF and air dried. Then all the crystals were transferred to a 20 mL scintillation vial and solvent exchange was done with $CH_2Cl_2$by leaving the crystals in 15 mL $CH_2Cl_2$for 24 h. The single crystalline nature of the sample was lost after the solvent exchange. Polycrystalline powder was filtered and again washed with CH_2Cl_2. The powder was then transferred to a vial and activated at 150 °C under dynamic vacuum. The desired structure and phase transition is confirmed by PXRD measurements (Fig. S4). Complete solvent (DMF) removal from the system is confirmed by the ^{1}H NMR spectroscopy in DMSO-d_6 and trifluoroacetic acid-d_1 (Fig. S5–6).

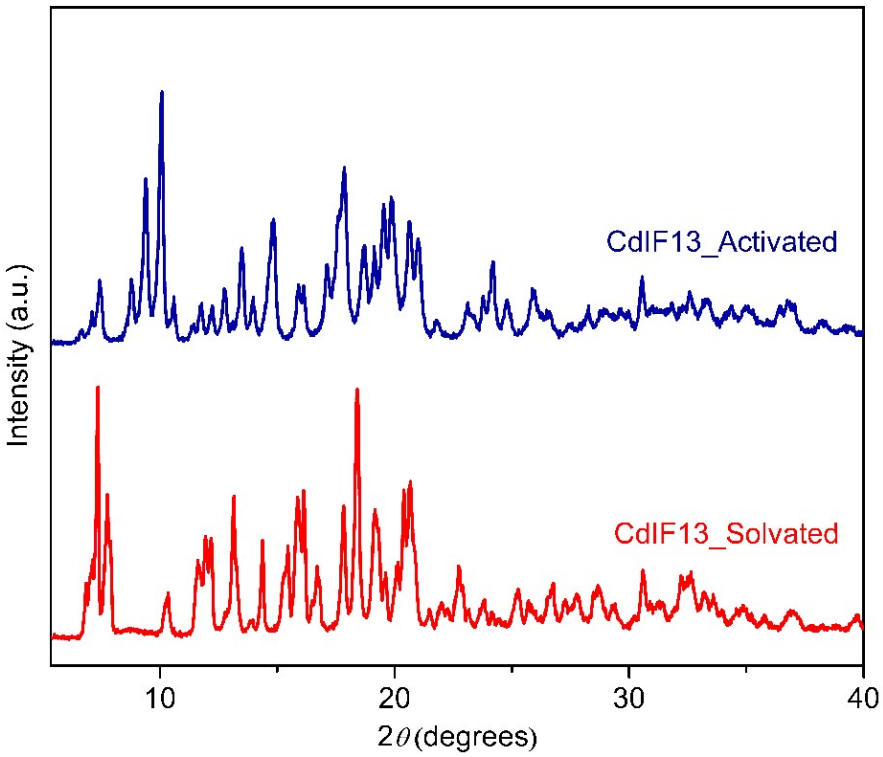

Fig. S4. Powder X-ray diffraction pattern of *N,N*-dimethylformamide-solvated CdIF-13 (bottom, red) and activated CdIF-13 (top, blue) collected under ambient conditions.

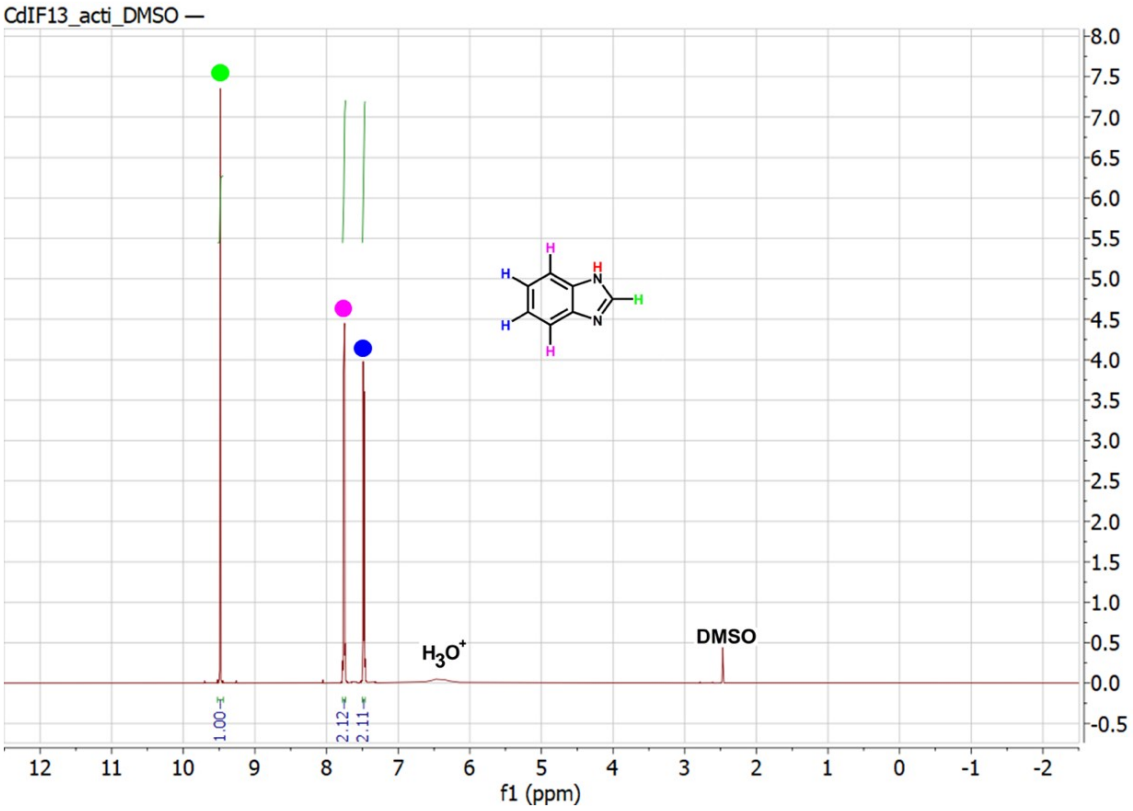

Fig. S5. ^{1}H NMR spectrum of digested activated CdIF-13 (~10 mg in 0.1 mL 35% DCl in D_2O and 0.6 mL DMSO–d_6. 500 MHz).

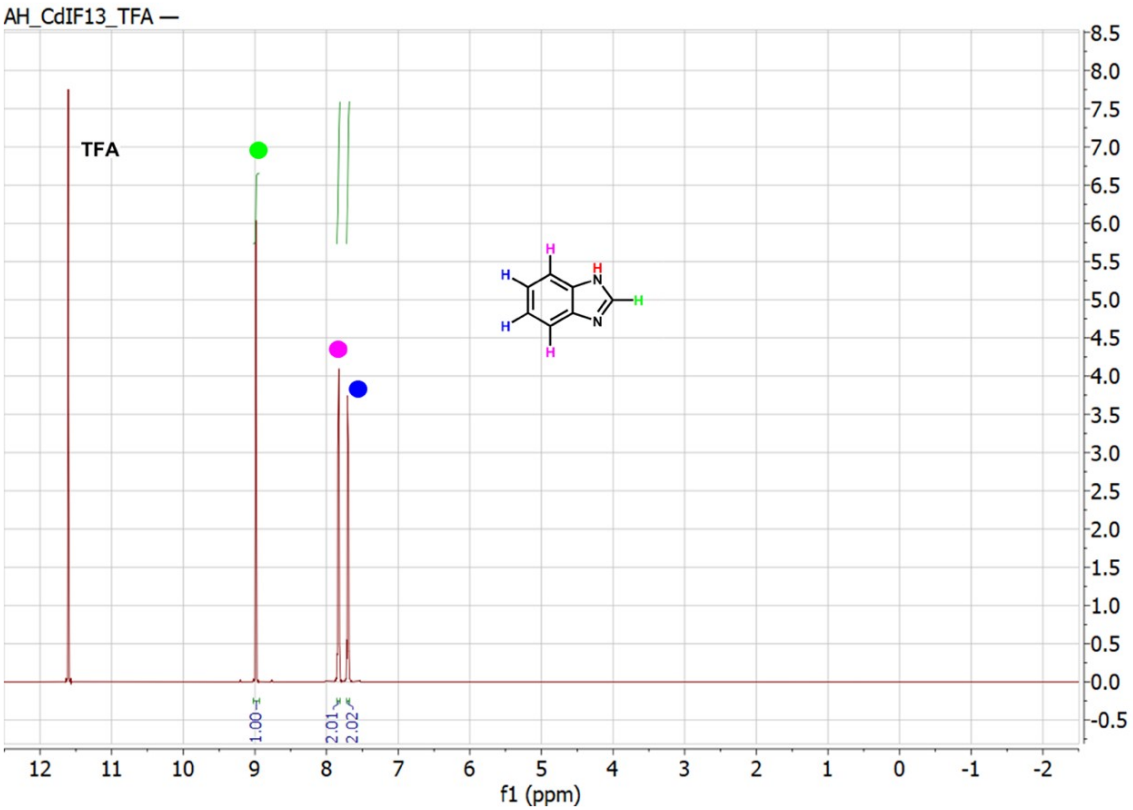

Fig. S6. ^{1}H NMR spectrum of activated CdIF-13 (~10 mg in 0.7 mL trifluoroacetic acid–d_1. 500 MHz).

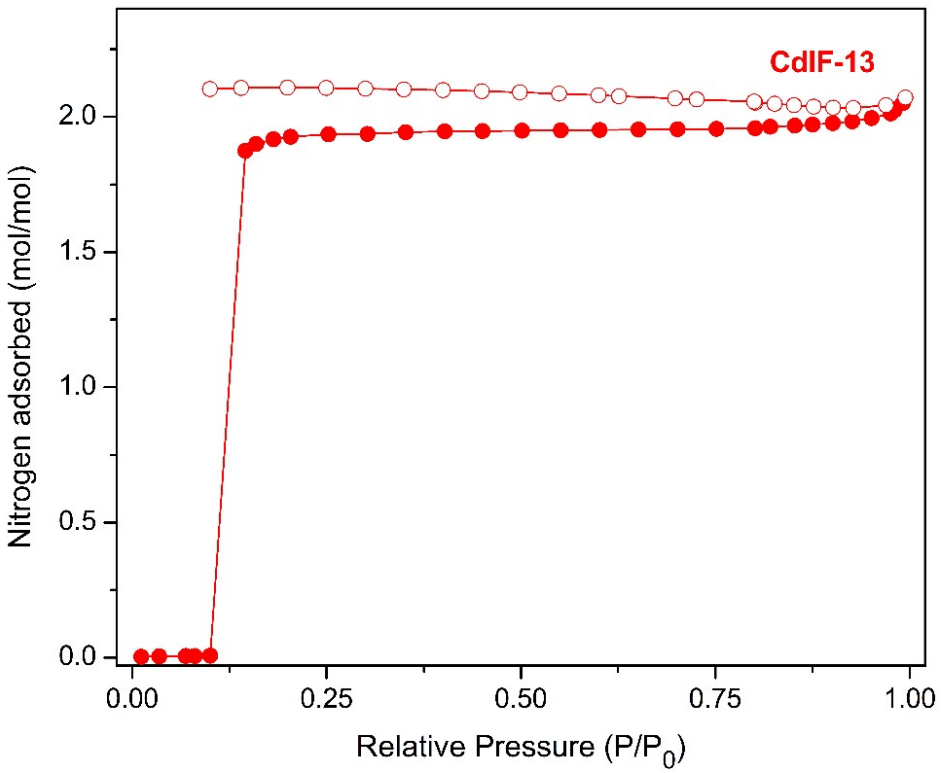

Fig. S7. Nitrogen adsorption isotherm for CdIF-13 collected at 77 K. Filled and unfilled circle represent adsorption and desorption respectively. The lines connecting data points are only to guide the eye and are not mathematical fits.

Synthesis and activation of multi-variate MOFs.

A similar procedure as the CdIF-13 was followed for the synthesis and activation of the multivariate MOF materials. The only difference was that the second ligand 2-methyl-5,6-difluorobenzimidazole (2M56DFbim) was used along with benzimidazole in different ratios. An example synthetic procedure is as follows

In a 4 mL scintillation vial, $Cd(ClO_4)_2 \cdot xH_2O$ (300 mg) in a total of 2 mL DMF was mixed with different ratios of benzimidazole and 2-methyl-5,6-difluorobenzimidazole as presented in Table 1, giving the same total mmol of ligand (i.e., 1 mmol total) as used in the synthesis of CdIF-13, and placed in an oven at 130 °C. After 72 h, the vials were slowly cooled to room temperature by shutting down the oven with the door closed. Magenta-color crystalline or micro crystalline multi-variate MOFs are found along the walls of the vials. Samples were collected by filtration and washed with excess DMF to remove any starting ingredients. The sample were then thoroughly washed with CH_2Cl_2 to remove the excess DMF and dried on the filter. The single crystalline nature of the samples was lost after the CH_2Cl_2 wash, turning them polycrystalline. The polycrystalline materials were transferred to 20 mL scintillation vials and solvent exchange with CH_2Cl_2 was done by adding the crystalline materials to 15 mL CH_2Cl_2 for 24h. The polycrystalline powder was filtered and again washed with CH_2Cl_2. The powder was then transferred to a vial and activated at 150 °C under dynamic vacuum. The desired structure and reversable phase transition is confirmed by PXRD measurements (Fig. S8–13). Complete solvent (DMF) removal from the system is confirmed by the ^{1}H NMR spectroscopy in trifluoroacetic acid-d_1 (Fig. S17–22) except the 5:4 MOF, where 0.02 equivalent of DMF is trapped even after the above-mentioned washing, solvent exchange, and activation procedure. The ligand ratio in the individual synthesized multivariate frameworks was determined from the NMR spectra of the digested frameworks. Relative air stability of these multivariate systems was confirmed for one of the representative MOF by PXRD measurements under air-free condition (Fig. S15) and IR spectroscopic study (Fig. S16).

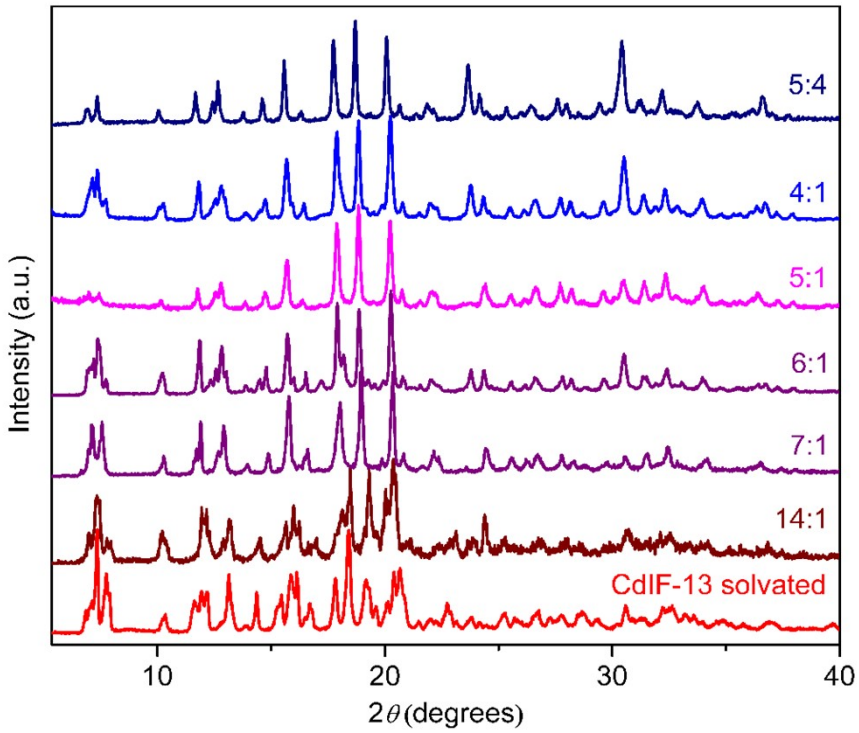

Fig. S7. Powder X-ray diffraction pattern of all the as-synthesized, *N,N*-dimethylformamide-solvated multivariate MOFs with the base MOF CdIF-13. These patterns were collected under ambient condition.

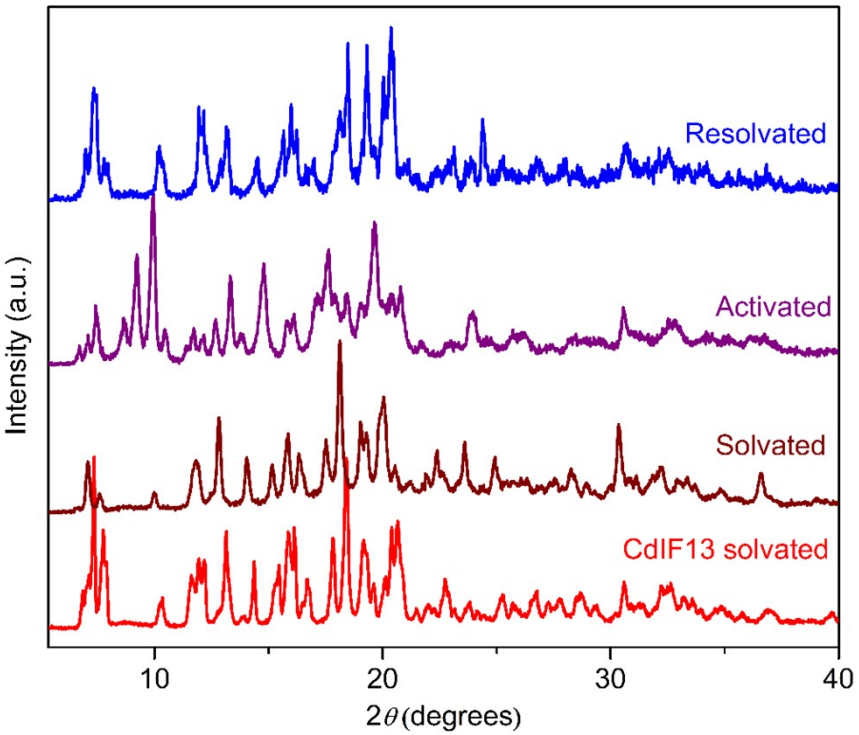

Fig. S8. Powder X-ray diffraction pattern of as-synthesized, *N,N*-dimethylformamide-solvated CdIF-13 (red), as-synthesized *N,N*-dimethylformamide-solvated 14:1 MOF (brown), activated 14:1 MOF (purple), and *N,N*-dimethylformamide re-solvated 14:1 MOF (blue) collected under ambient conditions.

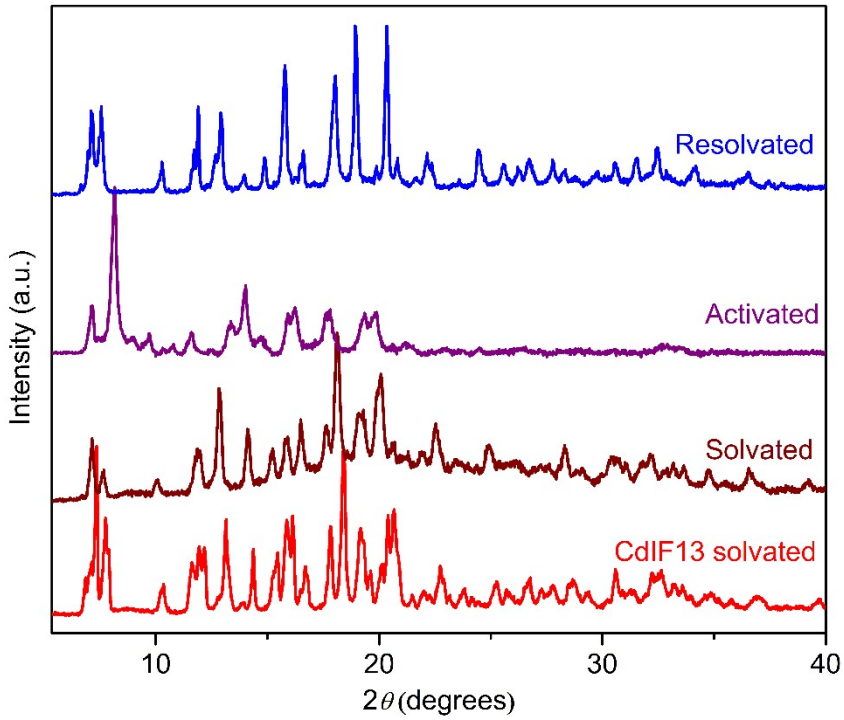

Fig. S9. Powder X-ray diffraction pattern of *N,N*-dimethylformamide-solvated CdIF-13 (red), as-synthesized *N,N*-dimethylformamide-solvated 7:1 MOF (brown), activated 7:1 MOF (purple), and *N,N*-dimethylformamide re-solvated 7:1 MOF (blue) collected under ambient conditions.

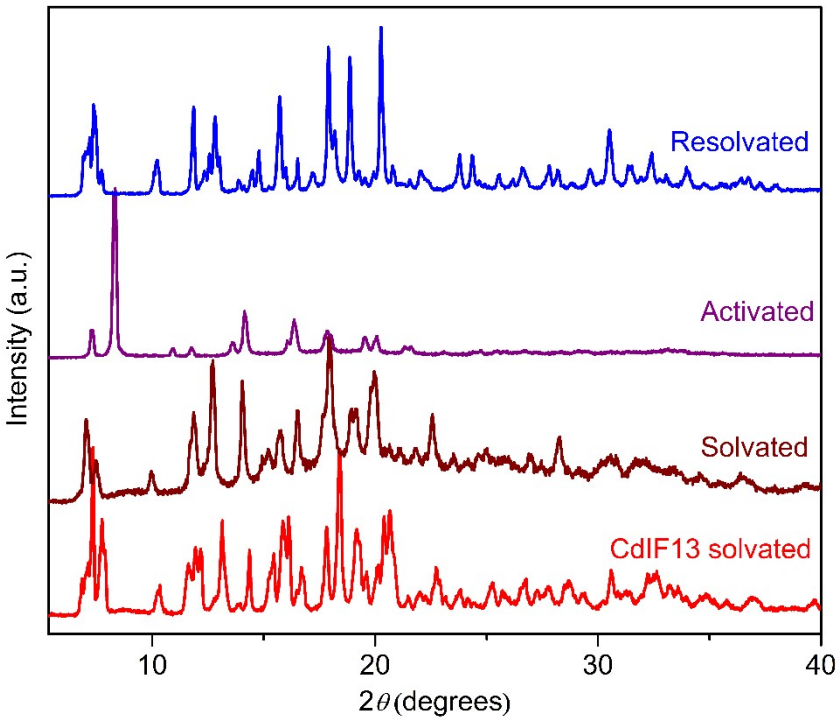

Fig. S10. Powder X-ray diffraction pattern of *N,N*-dimethylformamide-solvated CdIF-13 (red), as-synthesized *N,N*-dimethylformamide-solvated 6:1 MOF (brown), activated 6:1 MOF (purple), and *N,N*-dimethylformamide re-solvated 6:1 MOF (blue) collected under ambient conditions.

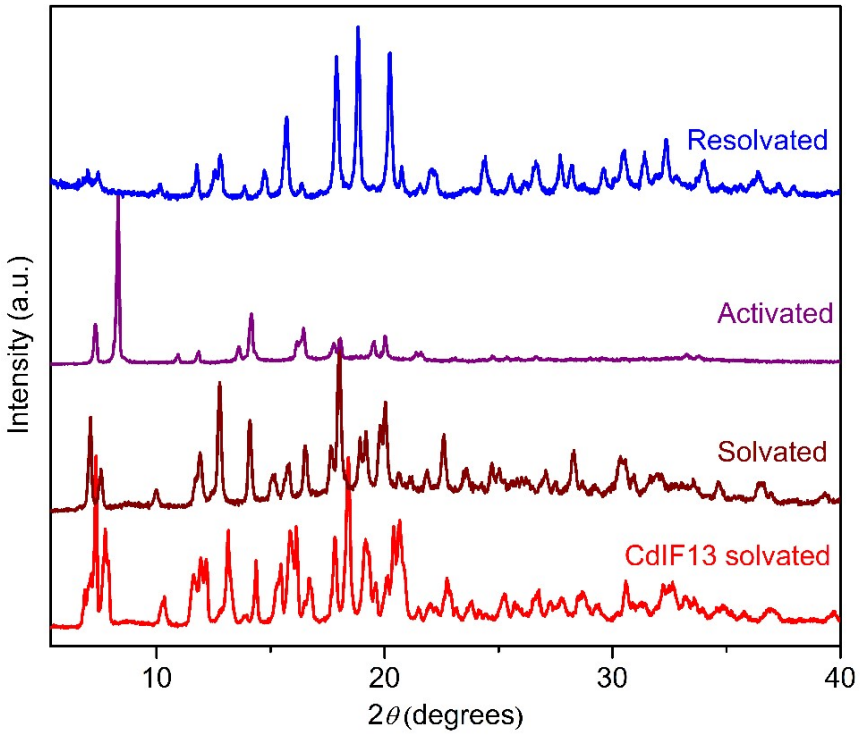

Fig. S11. Powder X-ray diffraction pattern of *N,N*-dimethylformamide-solvated CdIF-13 (red), as-synthesized *N,N*-dimethylformamide-solvated 5:1 MOF (brown), activated 5:1 MOF (purple), and *N,N*-dimethylformamide re-solvated 5:1 MOF (blue) collected under ambient conditions.

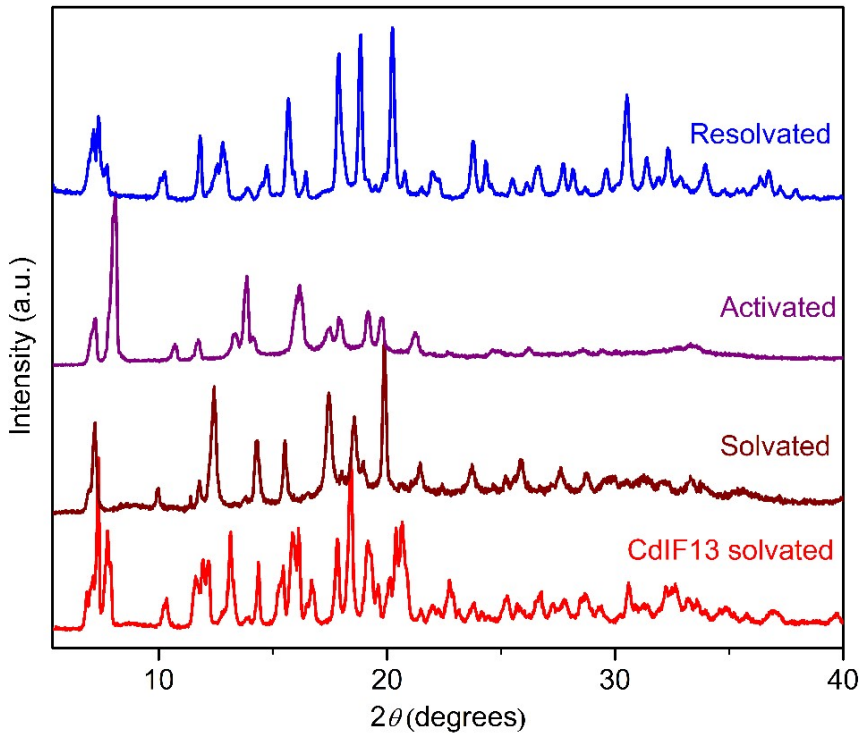

Fig. S12. Powder X-ray diffraction pattern of *N,N*-dimethylformamide-solvated CdIF-13 (red), as-synthesized *N,N*-dimethylformamide-solvated 4:1 MOF (brown), activated 4:1 MOF (purple), and *N,N*-dimethylformamide re-solvated 4:1 MOF (blue) collected under ambient conditions.

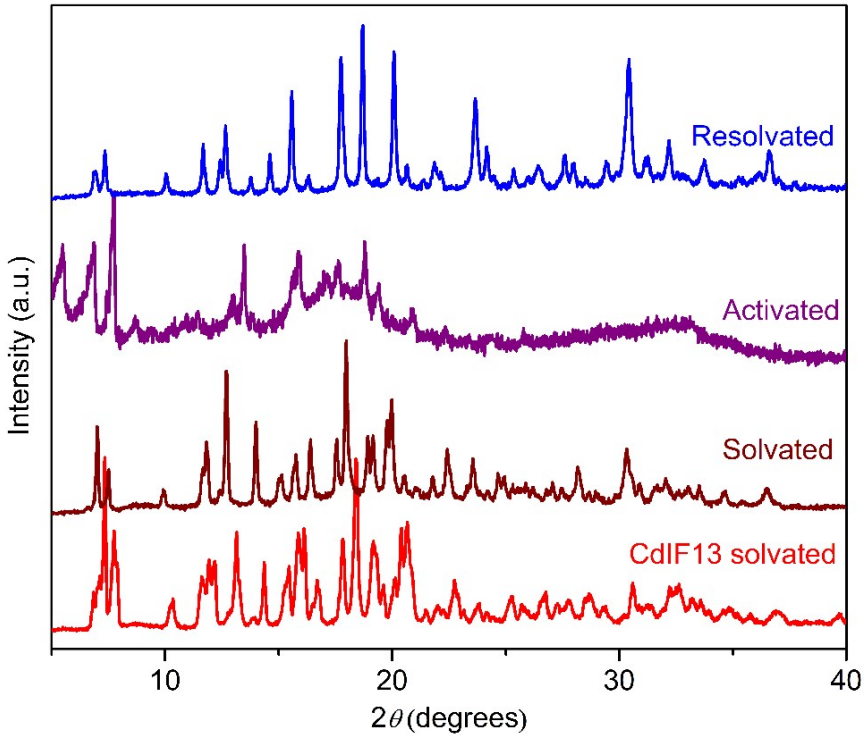

Fig. S13. Powder X-ray diffraction pattern of *N,N*-dimethylformamide-solvated CdIF-13 (red), as-synthesized *N,N*-dimethylformamide-solvated 5:4 MOF (brown), activated *N,N*-dimethylformamide re-solvated 5:4 MOF (purple), and 5:4 MOF (blue) collected under ambient conditions.

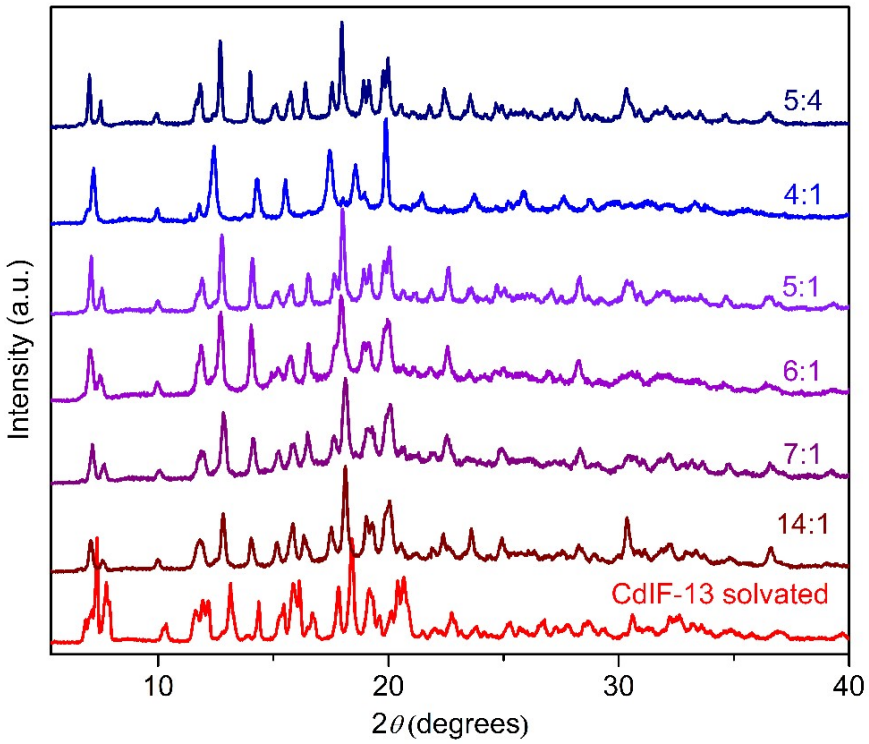

Fig. S14. Powder X-ray diffraction pattern of all the *N,N*-dimethylformamide re-solvated multivariate MOFs with the base MOF CdIF-13, collected under ambient conditions.

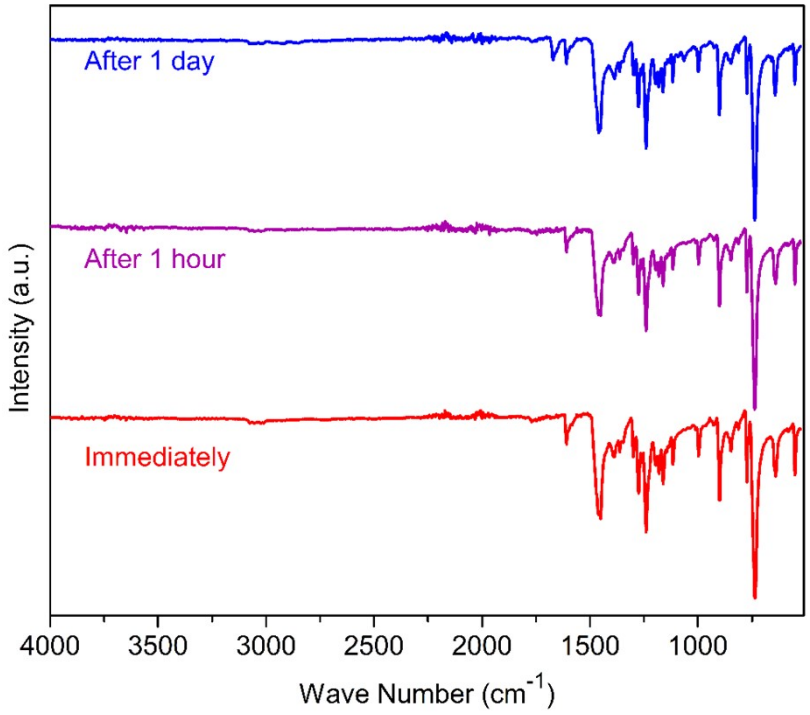

Fig. S15. FTIR data at room temperature for activated 7:1 MOF collected immediately removing from an inert atmosphere (red), activated 7:1 MOF collected after 1 h (after ambient condition PXRD data collection) (purple) and activated 7:1 MOF collected after 1 day air expose (blue).

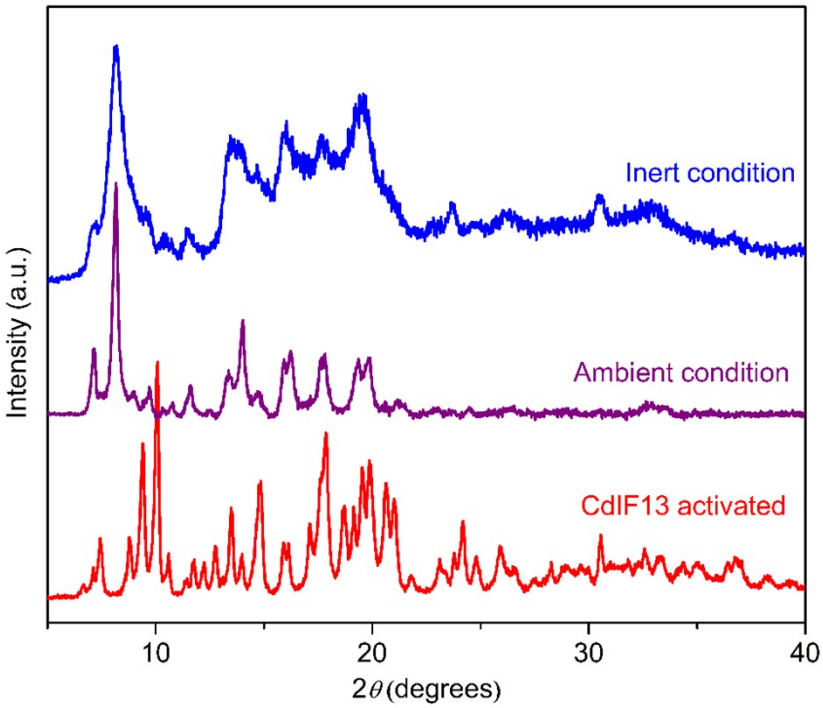

Fig. S16. Powder X-ray diffraction pattern of activated 7:1 MOF collected under inert atmosphere (blue), same sample on same sample holder after exposing to the ambient environment (purple) and activated CdIF-13 (red) at room temperature. The high background intensity for the data taken in the inert atmosphere is due to use of the air-free dome to maintain the inert atmosphere for the sample.

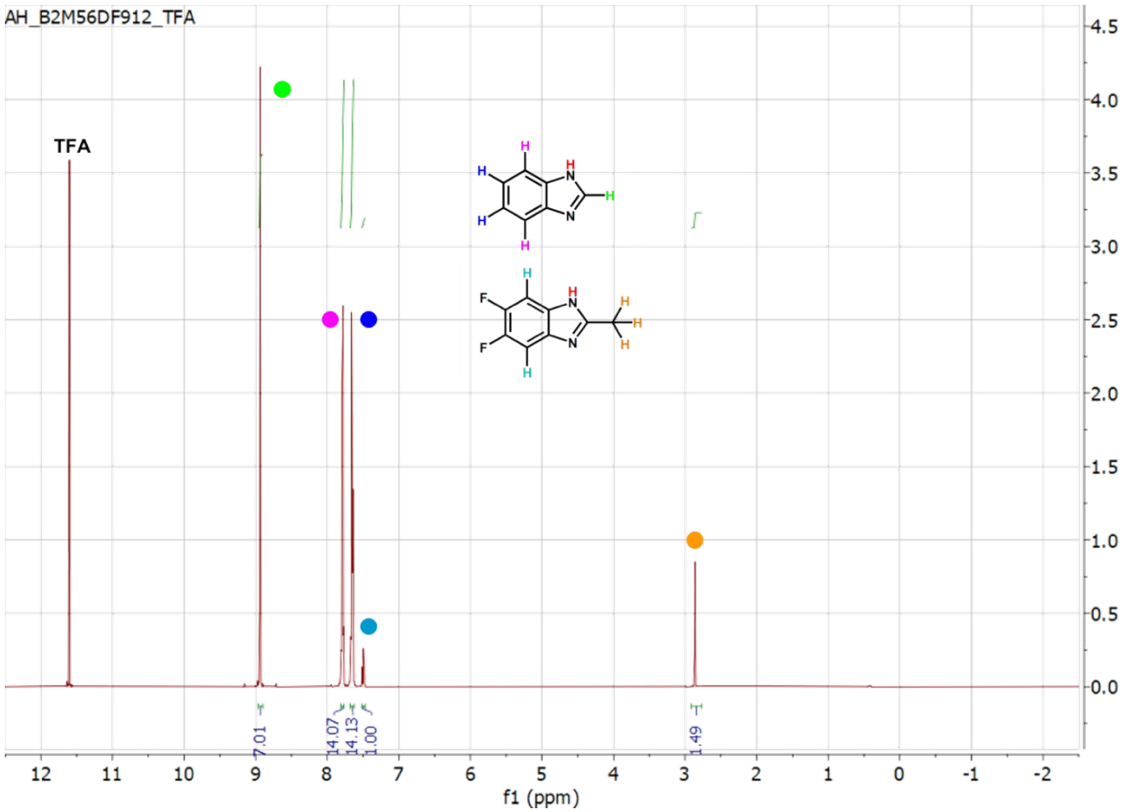

Fig. S17. ^{1}H NMR spectrum of activated 14:1 MOF (~10 mg in 0.7 mL trifluoroacetic acid–d_1. 500 MHz).

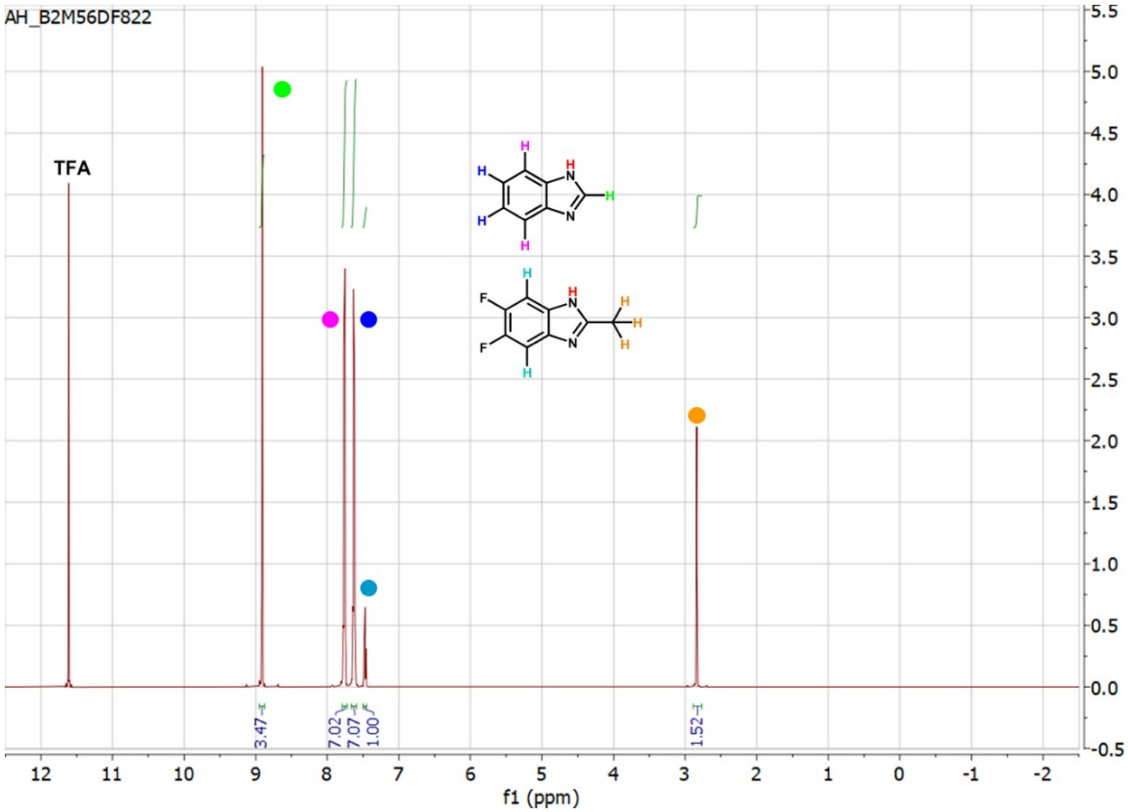

Fig. S18. ^{1}H NMR spectrum of activated 7:1 MOF (~10 mg in 0.7 mL trifluoroacetic acid–d_1. 500 MHz).

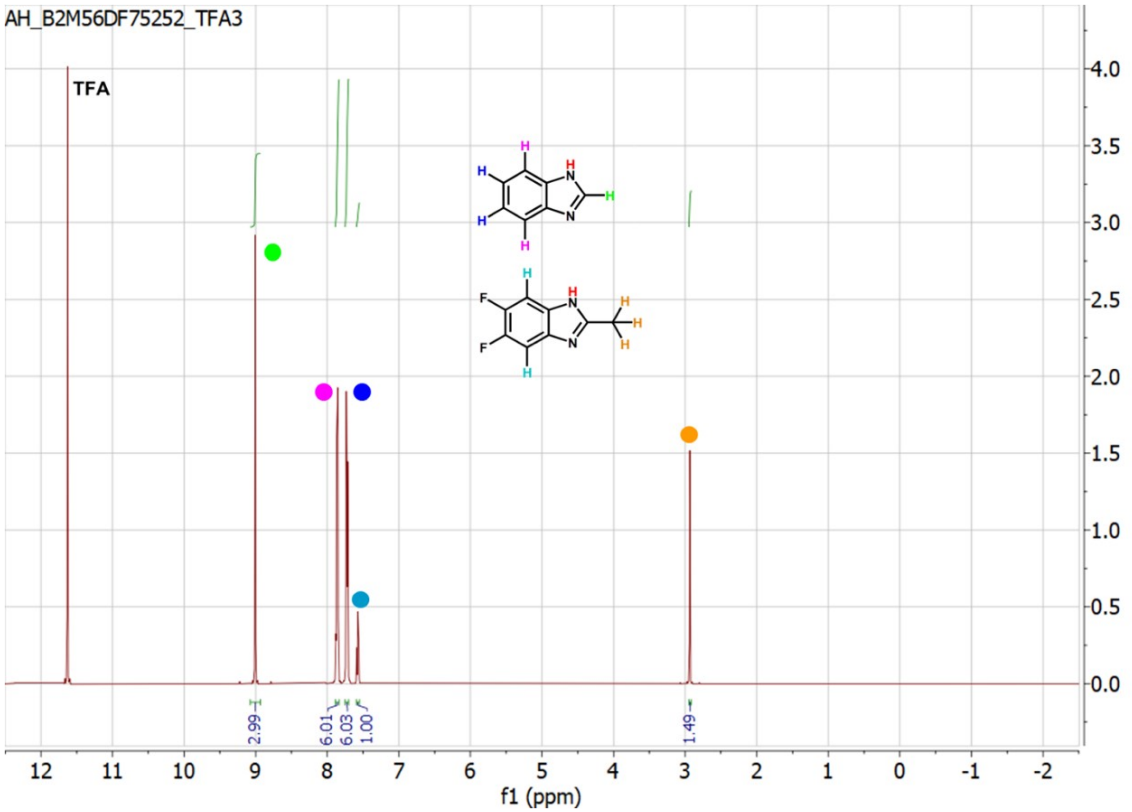

Fig. S19. ^{1}H NMR spectrum of activated 6:1 MOF (~10 mg in 0.7 mL trifluoroacetic acid–d_1. 500 MHz).

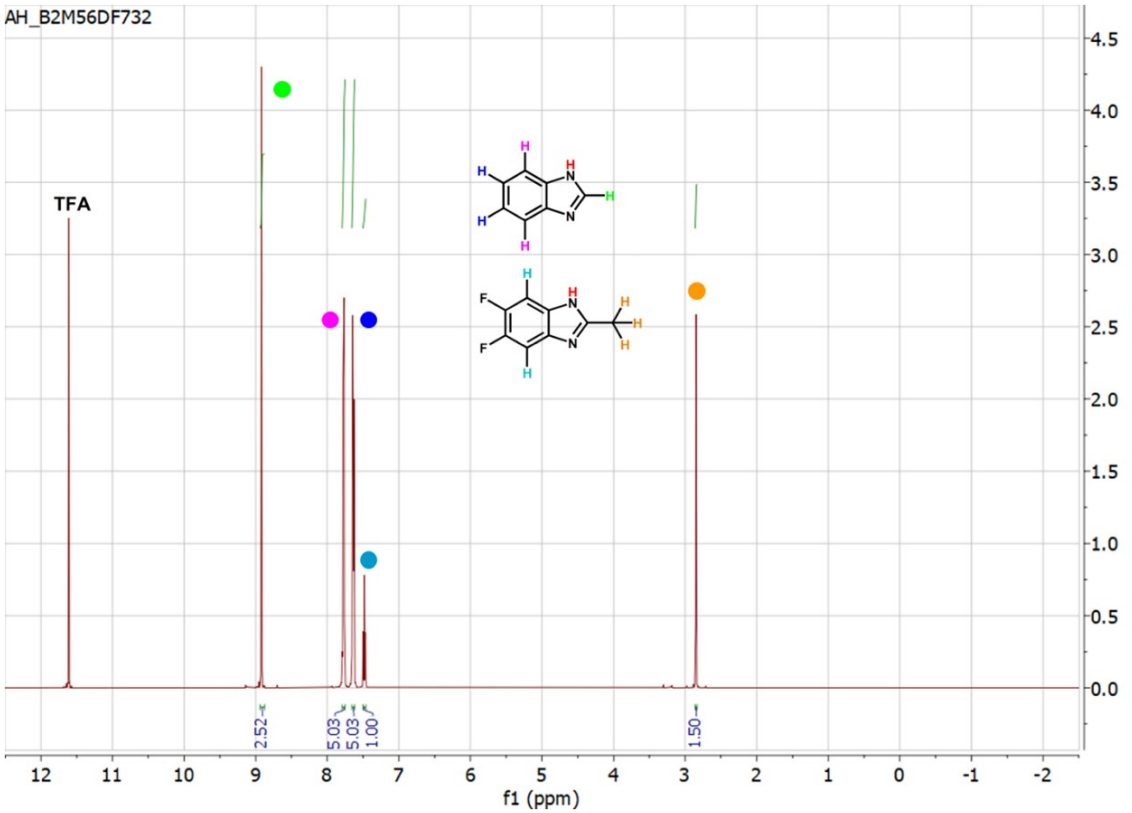

Fig. S20. ^{1}H NMR spectrum of activated 5:1 MOF (~10 mg in 0.7 mL trifluoroacetic acid–d_1. 500 MHz).

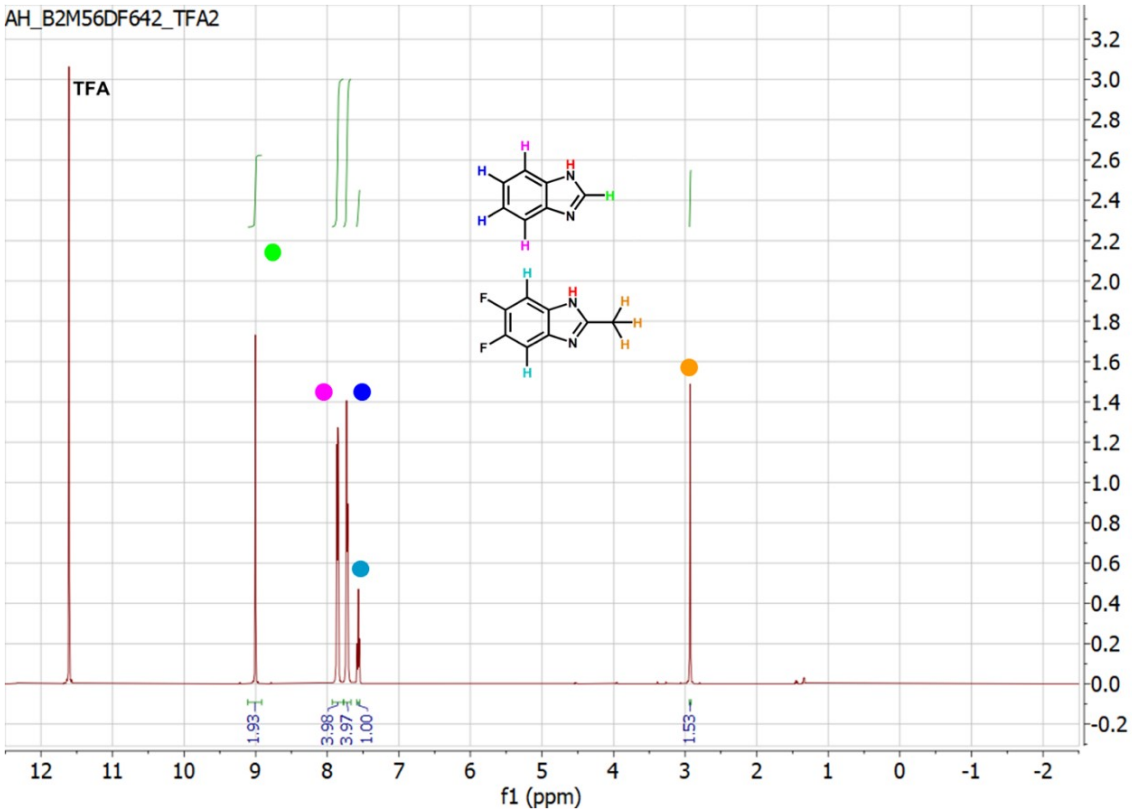

Fig. S21. ^{1}H NMR spectrum of activated 4:1 MOF (~10 mg in 0.7 mL trifluoroacetic acid–d_1. 500 MHz).

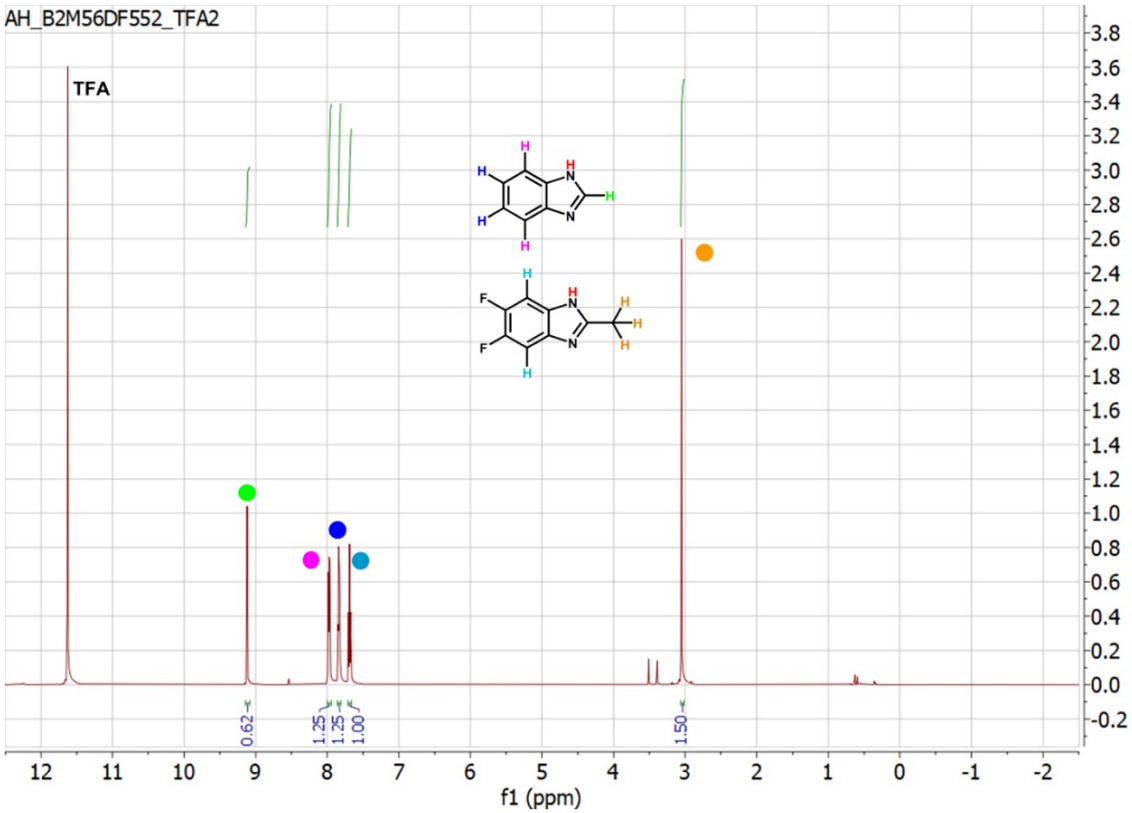

Fig. S22. ^{1}H NMR spectrum of activated 5:4 MOF (~10 mg in 0.7 mL trifluoroacetic acid–d_1. 500 MHz).

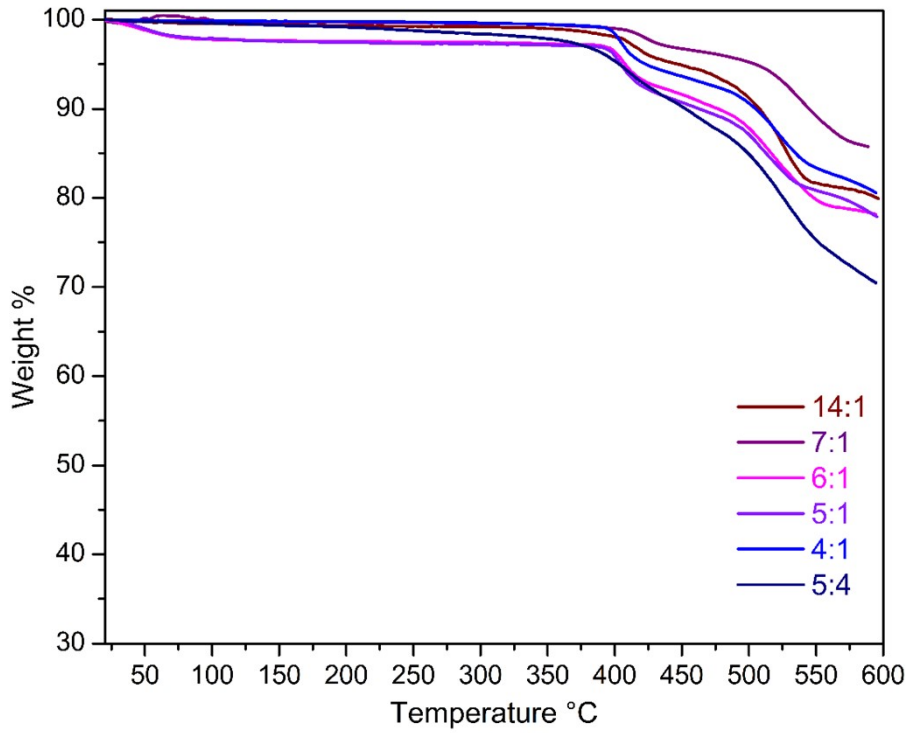

Fig. S23. Thermogravimetric analysis of activated MOFs. Thermogravimetric analysis was conducted using a TA instruments' TGA Q500 with a ramp rate of 5 °C min^{-1} to a final temperature of 600 °C under a nitrogen flow rate of 20 mL/min. Mass was uncorrected for buoyancy effects. Mass loss above 400 °C is likely due to framework thermal decomposition.

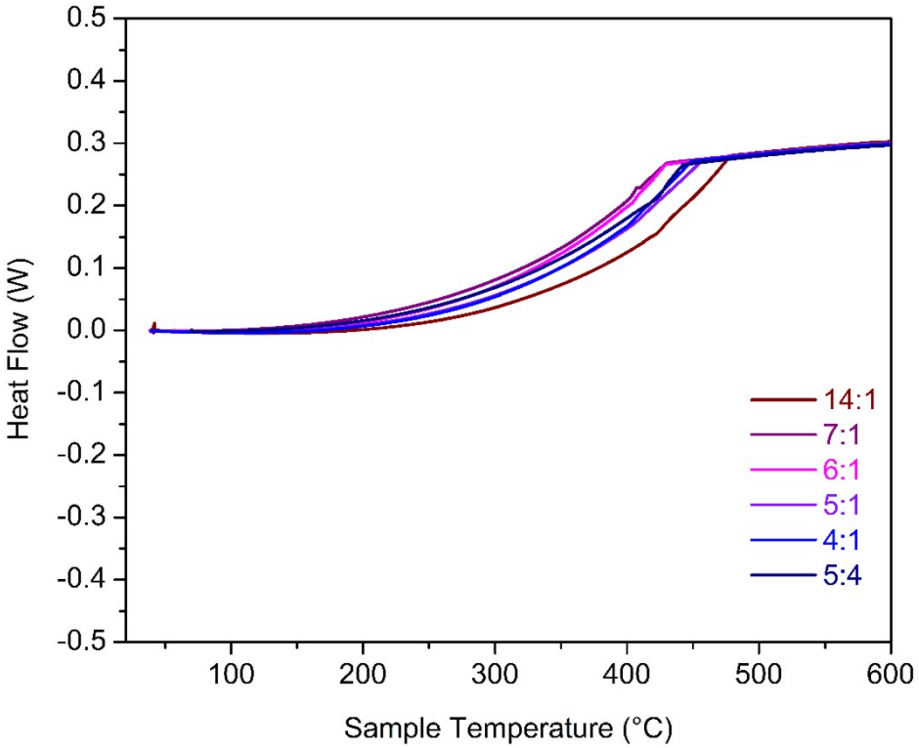

Fig. S24. Differential Scanning Calorimetry (DSC) decomposition of activated multivariate MOFs were studied using PerkinElmer's DSC8500 with a ramp rate of 5 °C min^{-1} to a final temperature of 600 °C under a nitrogen flow rate of 20 mL/min.

Gas Adsorption and Desorption Measurements

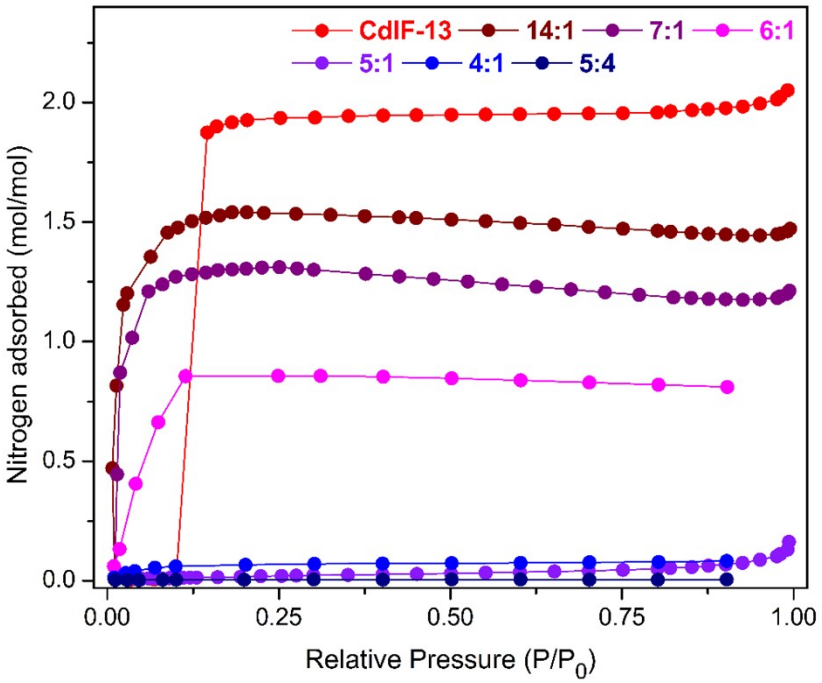

Fig. S25. Nitrogen adsorption isotherm curves for CdIF-13 and multivariate MOFs collected at 77 K. The observed minimal adsorption for 5:1, 4:1 and 5:4 frameworks is most likely due to the high pressure needed to induce the phase change concomitant with stepped adsorption. This is in line with the observed trends in adsorption threshold pressure with propane. The lines connecting data points are intended to guide the eye and are not mathematical fits. P_0 = 1 bar.

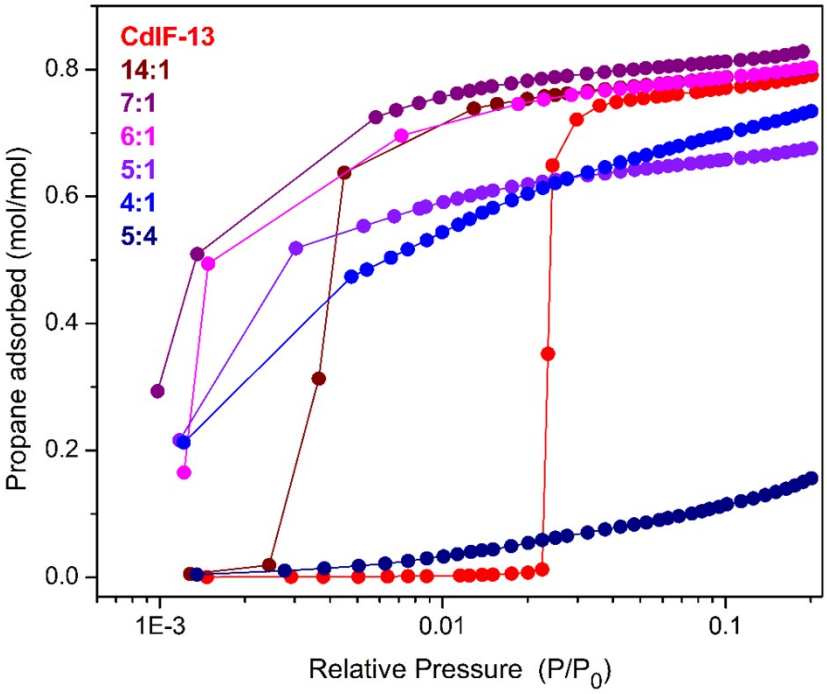

Fig. S26. Propane adsorption isotherms for multivariate MOFs collected at 4 °C. The lines connecting data points are only to guide the eye and are not mathematical fits. P_0 = 1 bar.

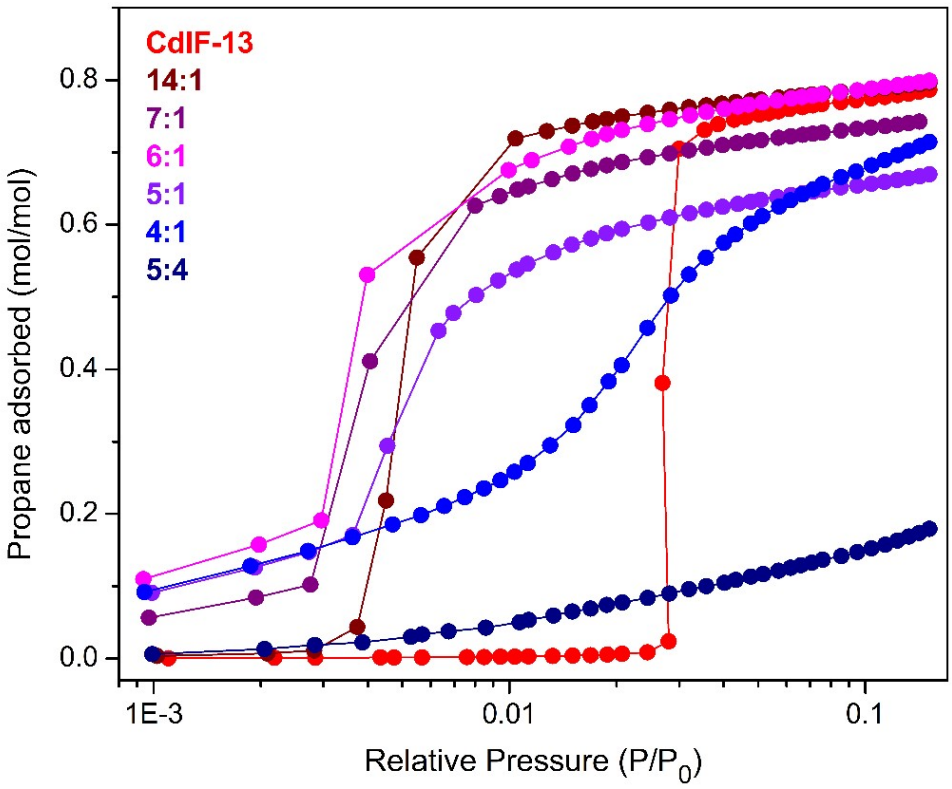

Fig. S27. Propane adsorption isotherms for multivariate MOFs collected at 14 °C. The lines connecting data points are only to guide the eye and are not mathematical fits. P_0 = 1 bar.

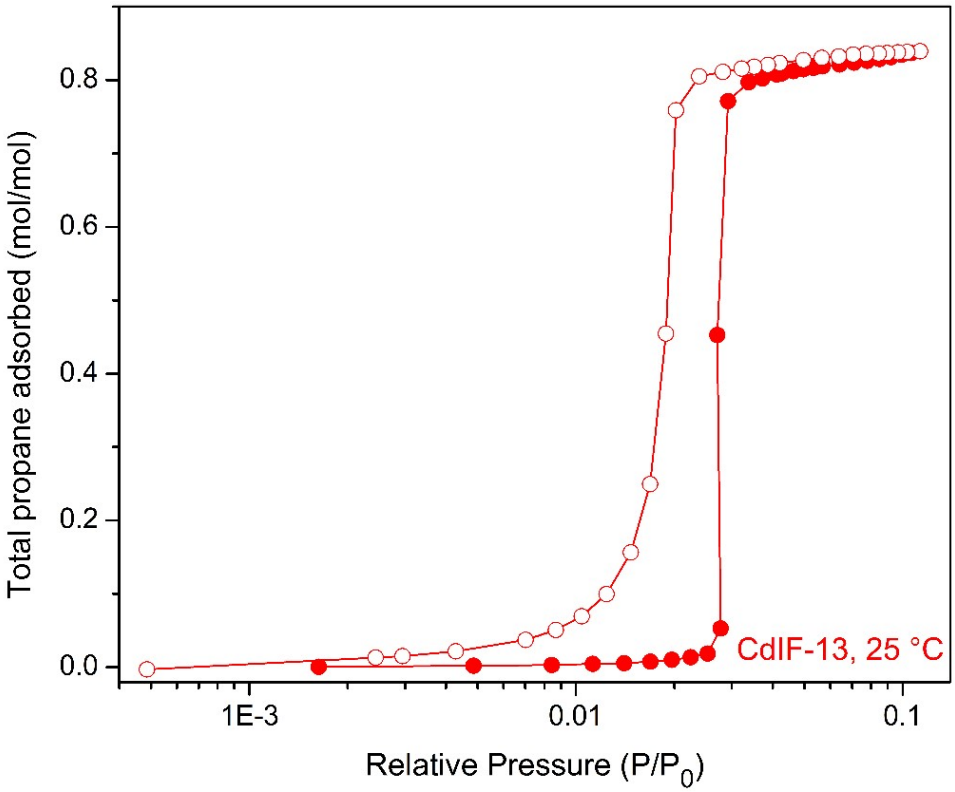

Fig. S29. Propane adsorption (closed circles) and desorption (open circles) isotherms for CdIF-13 MOF collected at 25 °C. The lines connecting data points are only to guide the eye and are not mathematical fits. P_0 = 1 bar

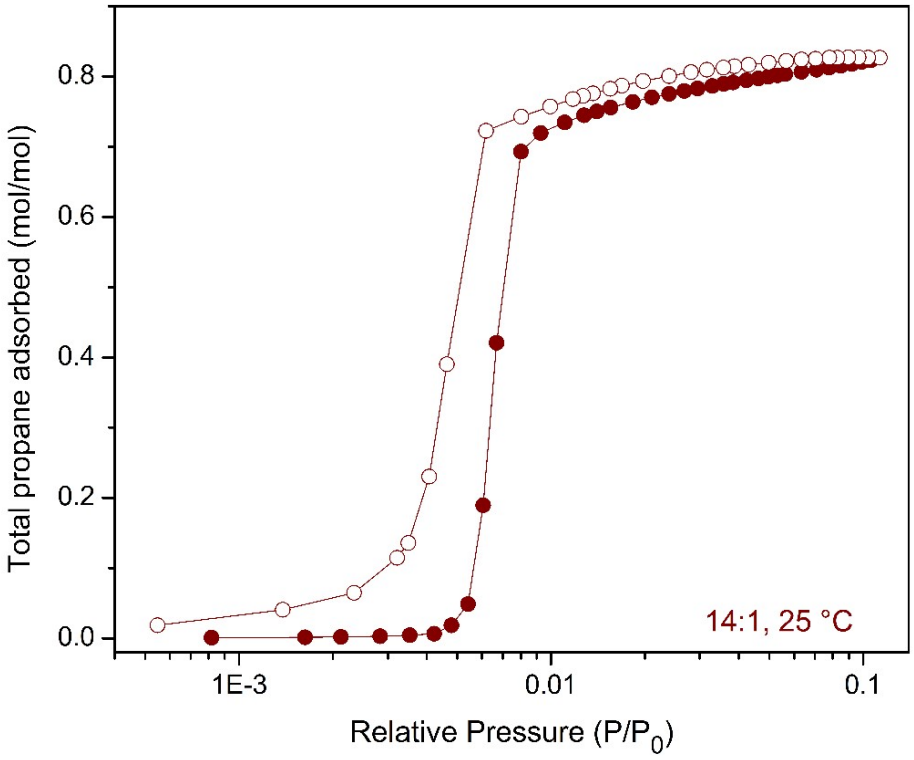

Fig. S29. Propane adsorption (closed circles) and desorption (open circles) isotherms for 14:1 MOF collected at 25 °C. The lines connecting data points are only to guide the eye and are not mathematical fits. P_0 = 1 bar

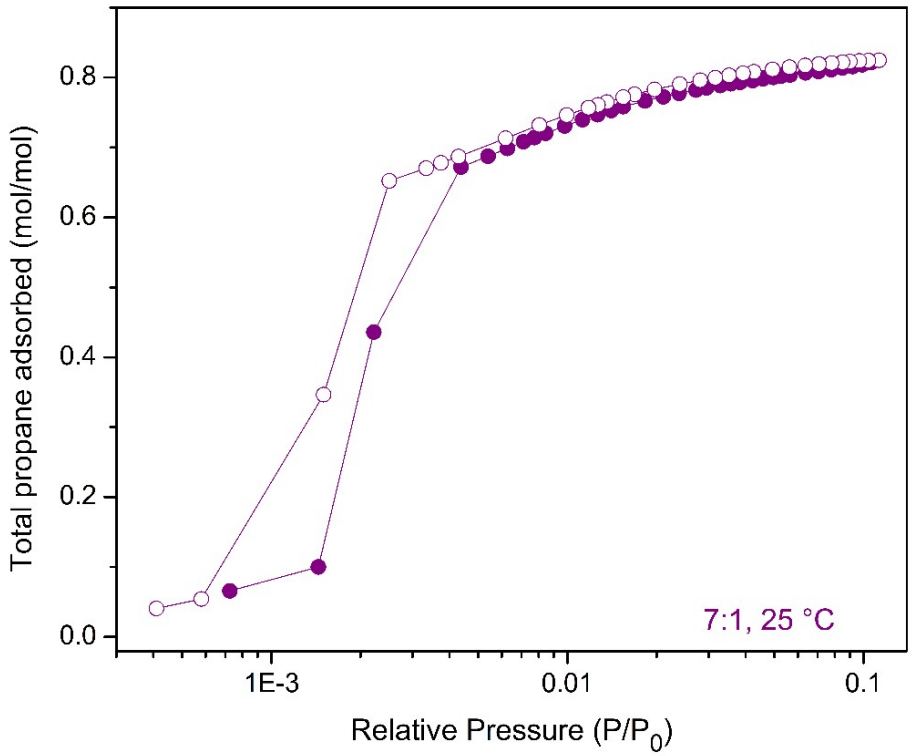

Fig. S31. Propane adsorption (closed circles) and desorption (open circles) isotherms for 7:1 MOF collected at 25 °C. The lines connecting data points are only to guide the eye and are not mathematical fits. P_0 = 1 bar

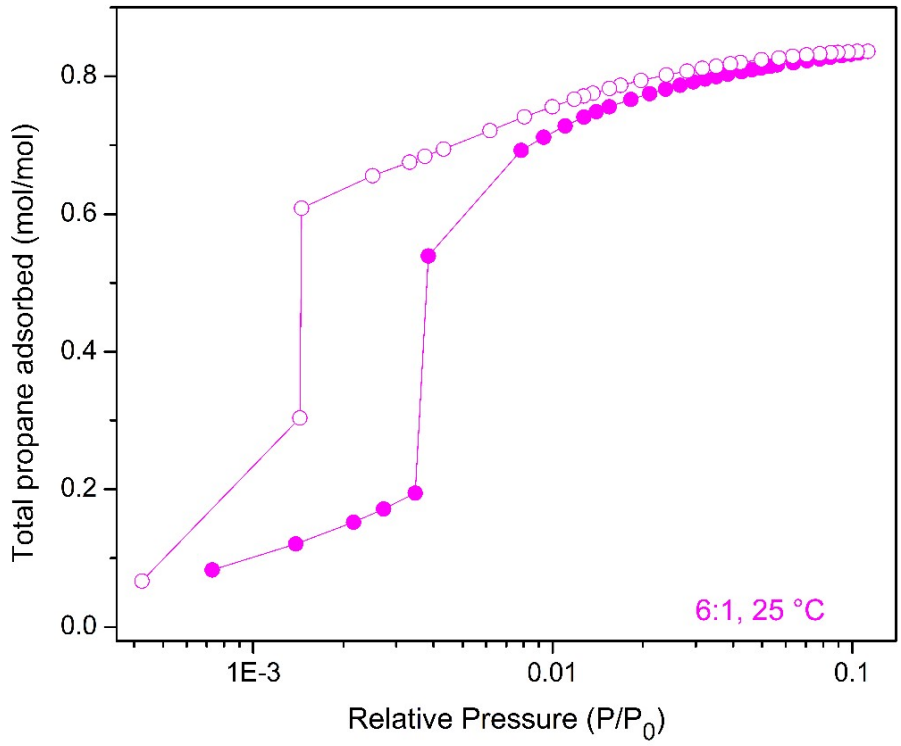

Fig. S32. Propane adsorption (closed circles) and desorption (open circles) isotherms for 6:1 MOF collected at 25 °C. The lines connecting data points are only to guide the eye and are not mathematical fits. P_0 = 1 bar

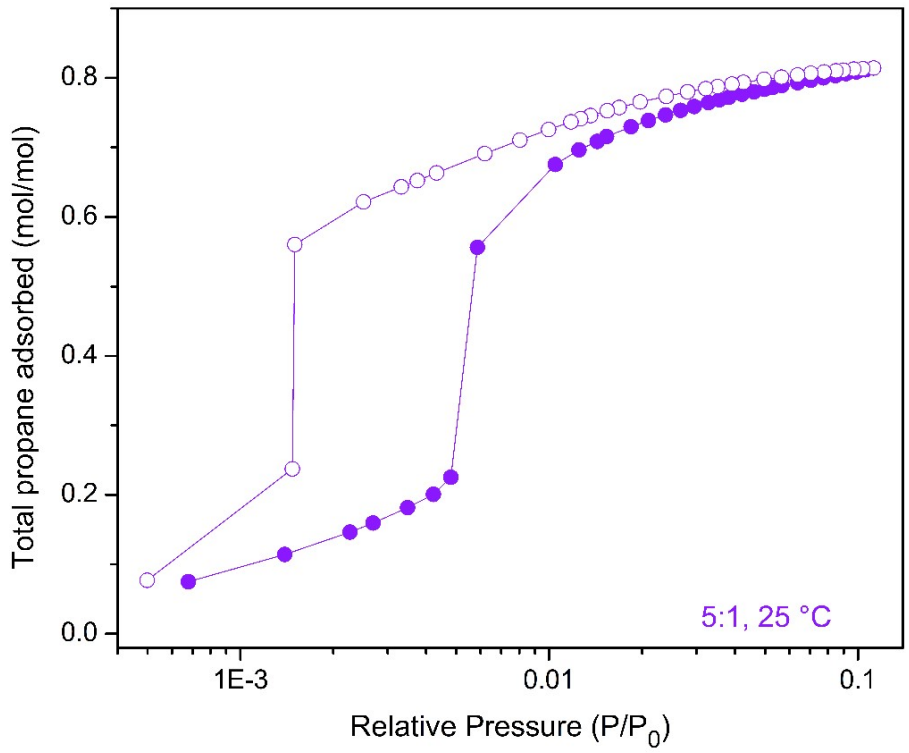

Fig. S33. Propane adsorption (closed circles) and desorption (open circles) isotherms for 5:1 MOF collected at 25 °C. The lines connecting data points are only to guide the eye and are not mathematical fits. P_0 = 1 bar

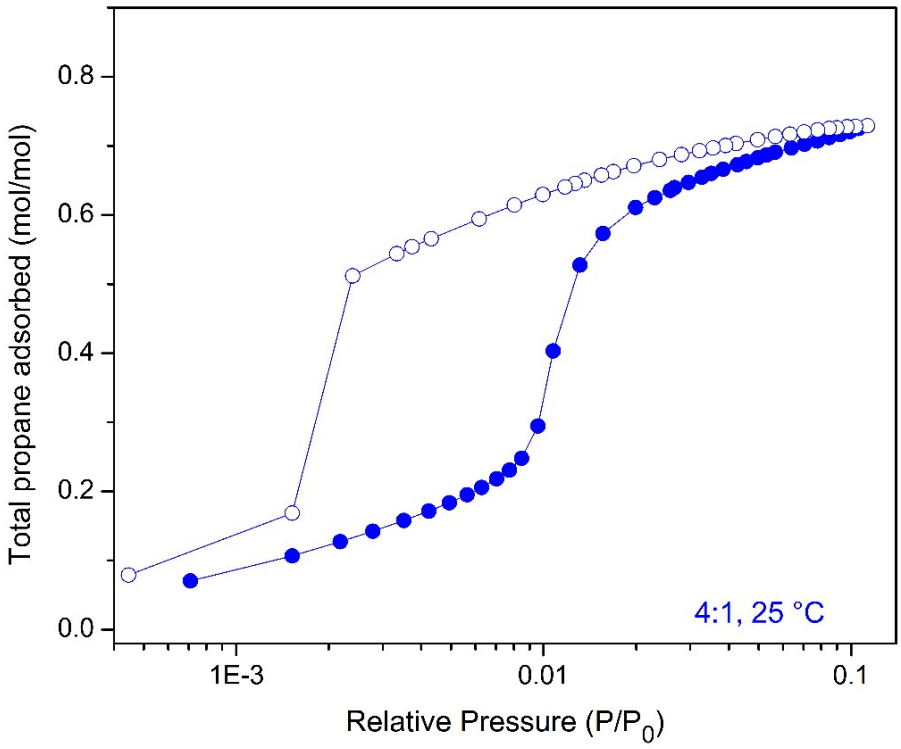

Fig. S34. Propane adsorption (closed circles) and desorption (open circles) isotherms for 4:1 MOF collected at 25 °C. The lines connecting data points are only to guide the eye and are not mathematical fits. P_0 = 1 bar

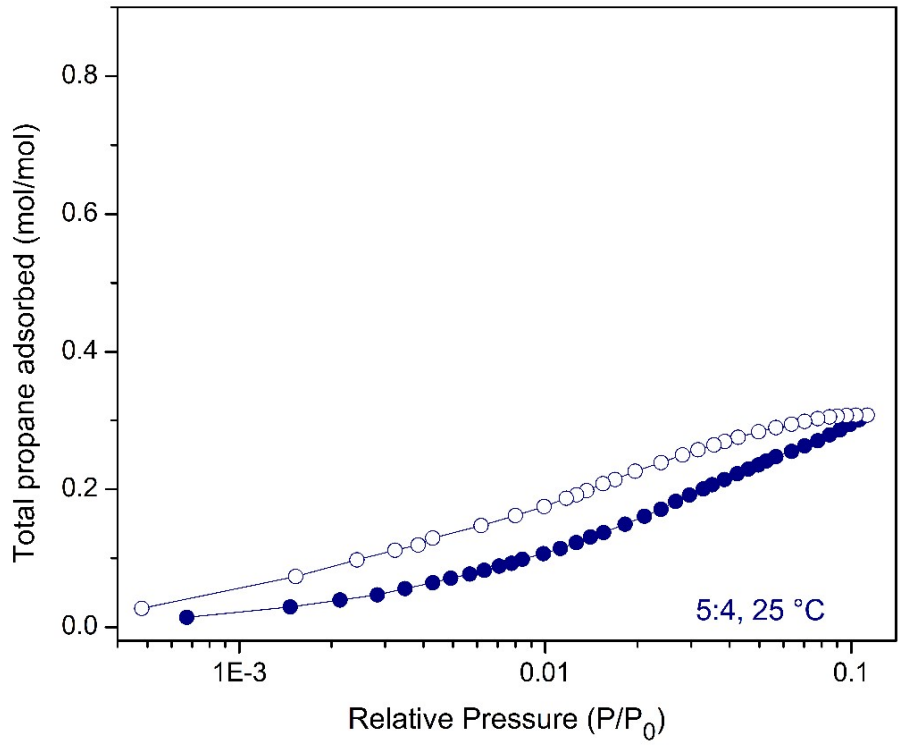

Fig. S35. Propane adsorption (closed circles) and desorption (open circles) isotherms for 5:4 MOF collected at 25 °C. The lines connecting data points are only to guide the eye and are not mathematical fits. P_0 = 1 bar.

Single-crystal X-ray Diffraction Studies

General refinement strategy

X-ray diffraction analysis was performed on good quality single crystals coated with Paratone-N oil and mounted on a mylar loop on a XtaLAB Synergy R, DW system, HyPix diffractometer. During data collection the crystal was kept at around 100 K under a flow of N_2 gas. Using Olex2,[3] the structures were solved with the SHELXT[4] structure solution program using Intrinsic Phasing and refined with the XL[5] refinement package using Least Squares minimization. For all the structures enhanced rigid-bond restraint (SHELX keyword RIGU)[6] was applied globally. Additionally, for 14:1 MOF, distance restraints were imposed on the n6 benzimidazole as well as restraints were applied on similar displacement amplitudes separated by less than 1.7 Ang. Thermal parameters were refined anisotropically for all the non-hydrogen atoms. All the hydrogen atoms were placed in their ideal position before final refinement. In all these structures, solvent molecules present in the framework could not be modeled. Significant electron density remained in the voids due to these disordered solvent molecules. The solvent masking procedure as implemented in Olex2 was used to remove the electronic contribution of solvent molecules from the refinement. As the exact solvent content is not known, only the atoms used in the refinement model are reported in the formula here. For 14:1 MOF total solvent accessible volume / cell = 1855.1 $Å^3$ [33.4%] with total electron count / cell = 446.4. For 5:1 MOF total solvent accessible volume / cell = 1830.6 $Å^3$ [33.4%] with total electron count / cell = 398.2.

Table S1. Crystallographic data.

MOF system	14:1	5:1
Formula	$C_{82.98}H_{48.94}Cd_6F_{1.96}N_{24}$	$C_{42.5875}H_{30}Cd_3F_{1.1775}N_{12}$
Formula weight	2093.80	1069.41
Temperature / K	99.99(18)	99.98(15)
Crystal system	monoclinic	monoclinic
Space group	*I*2/*m*	*I*2/*m*
a, *b*, *c* (Å)	16.2010(13), 23.0159(19), 16.2213(16)	16.0043(13), 23.0932(17), 16.3664(17)
α, β, γ (°)	90, 113.343(10), 90	90, 112.481(11), 90
Volume ($Å^{3)}$	5553.5(9)	5589.2(9)
Z	2	4
ρ_{calc} / mg mm^{-3}	1.252	1.271
μ / mm^{-1}	9.422	9.376
F(000)	2041	2096
2Θ range for data collection	6.526 to 156.076°	6.57 to 136.468°
Reflections collected	20592	14503
Independent reflections	5628	5047
R(int)	0.1822	0.0764
Data/restraints/parameters	5628/296/288	5047/329/297
Goodness-of-fit on F^2	1.335	1.138
R_1[a], wR_2[b] [I>2σ (I)]	0.1411, 0.3979	0.1087, 0.3121
R_1[a], wR_2[b] [all data]	0.1896, 0.4508	0.1418, 0.3411
Largest diff. peak/hole (e $Å^{-3}$)	1.278/-1.824	2.116/-0.790

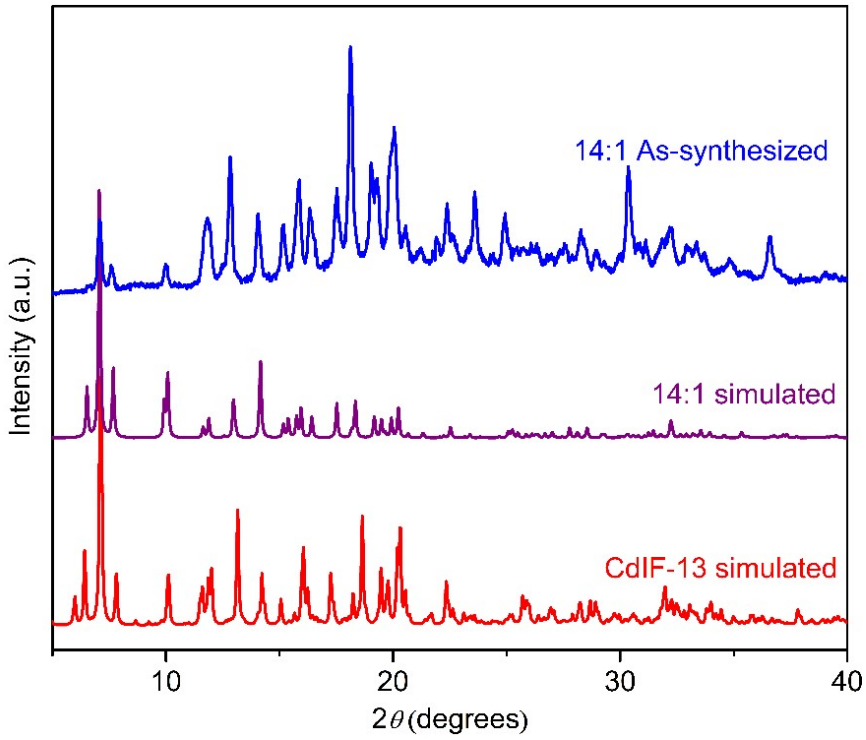

Fig. S36. Comparison of the PXRD pattern obtained for 14:1 bulk polycrystalline powder (top, blue) with pattern generated from the single crystal structure of DMF-solvated 14:1 system (middle, purple) and the DMF-solvated CdIF-13 (bottom, red) using Mercury CSD software.[7]

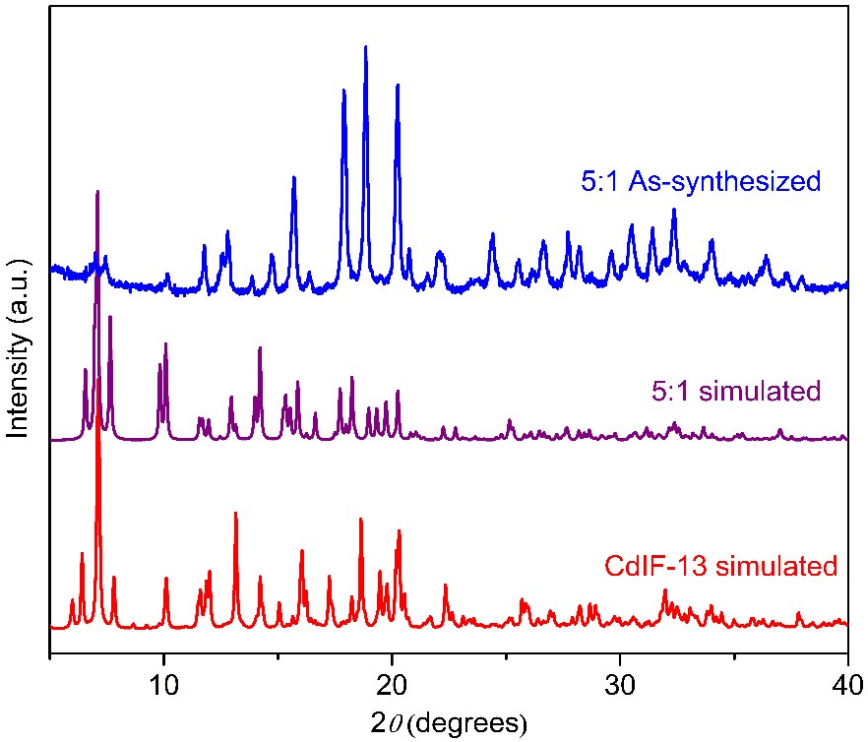

Fig. S37. Comparison of the PXRD pattern obtained for 5:1 bulk crystals (top, blue) with pattern generated from the single crystal structure of *N,N*-dimethylformamide- solvated 5:1 system (middle, purple) and the DMF-solvated CdIF-13 (bottom, red) using Mercury CSD software. [7]

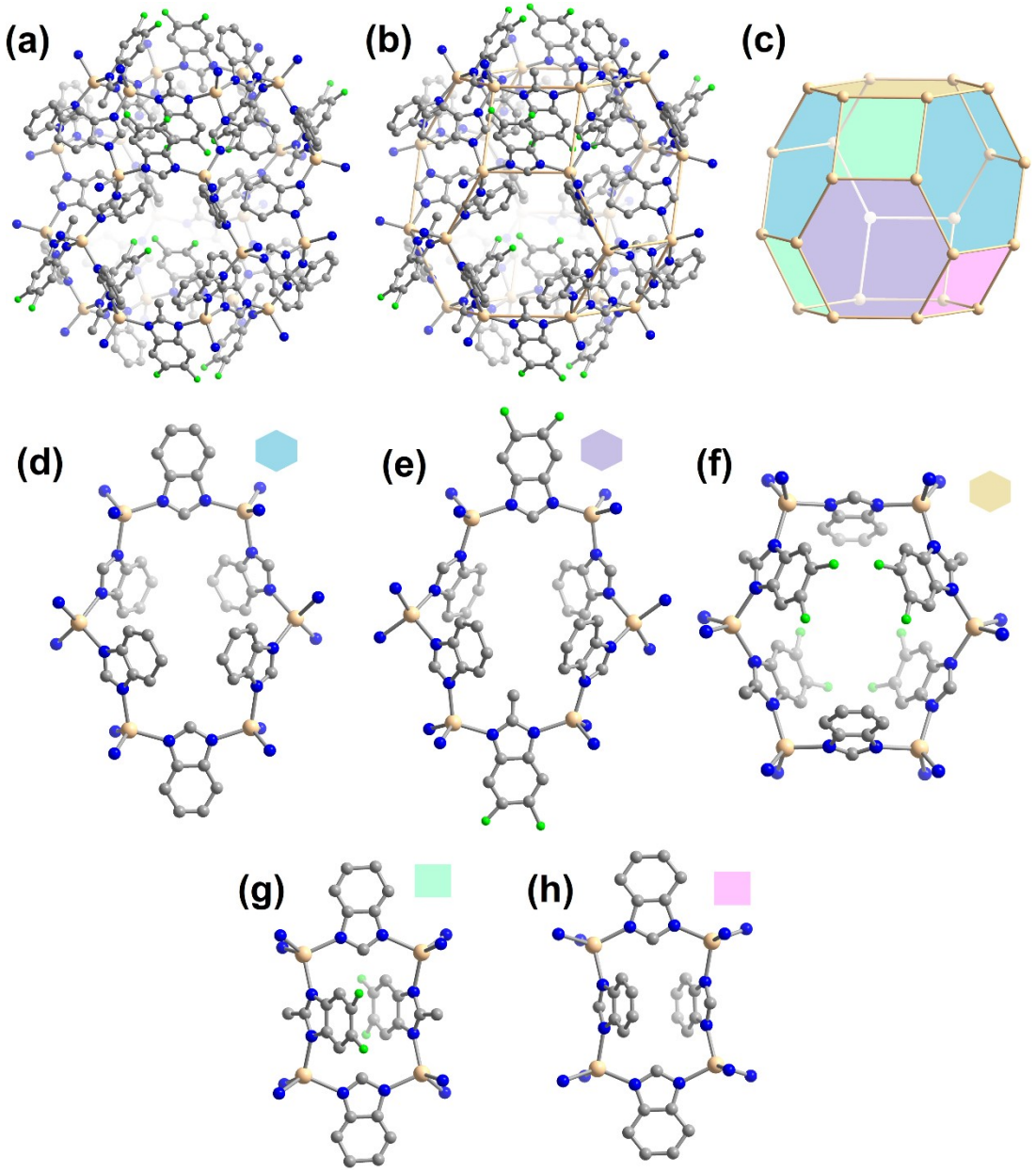

Fig. S38. Portions of the *N,N*-dimethylformamide-solvated structure for 14:1 MOF in the *I2/m* space group, are shown here. (a) Individual cage, found in the 14:1 system, is constructed by the Cd(II), bim$^-$ and 2M56DFbim$^-$ ligands. (b) Individual cage with the underlying skeleton of the structure present in the 14:1 system. (c) Sodalite-like topology is formed by the constituent skeleton of 4 and 6 membered rings. Different rings in the structure can be identified by colored polygons. (d) Blue hexagon represents the first 6-membered ring formed by only Cd(II) and bim ligand. (e) Second six membered ring is represented by purple hexagon and it is comprised of both bim$^-$ and 2M56DFbim$^-$ ligands along with Cd(II). (f) Third six membered ring is represented by yellow hexagon and it is also comprised of both bim$^-$ and 2M56DFbim$^-$ ligands along with Cd(II). (g) First 4 membered ring is represented by green rectangle and it formed by both bim$^-$ and 2M56DFbim$^-$ ligands along with Cd(II). (h) Second 4 membered ring is represented by magenta rectangle and it is formed by only bim$^-$ ligands along with Cd(II). Grey, dark blue, beige, and green spheres represent C, N, Cd, and F atoms, respectively; hydrogen atoms are omitted for clarity.

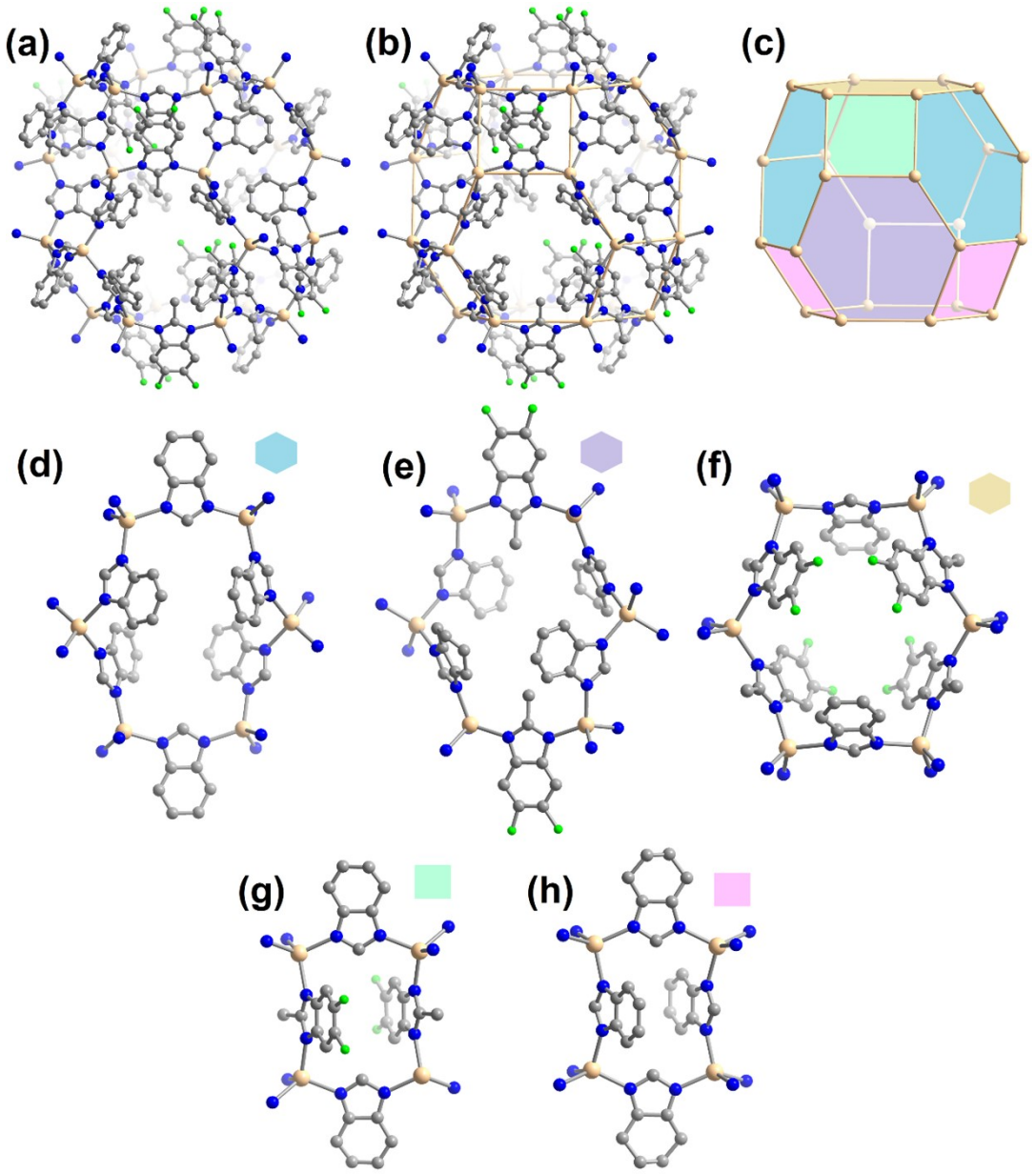

Fig. S39. Portions of the *N,N*-dimethylformamide-solvated structure for 5:1 MOF in the *I*2/*m* space group, are shown here. (a) Individual cage found in the 5:1 system, is constructed by the Cd(II), bim and 2M56DFbim ligands. (b) Individual cage with the underlying skeleton of the structure present in the 5:1 system. (c) Sodalite-like topology is formed by the constituent skeleton of 4 and 6 membered rings. Different rings in the structure can be identified by colored polygons. (d) Blue hexagon represents the first 6 membered ring formed by only Cd(II) and bim ligand. (e) Second 6 membered ring is represented by purple hexagon and it is comprised of both bim^- and $2M56DFbim^-$ ligands along with Cd(II). (f) Third 6 membered ring is represented by yellow hexagon and it is also comprised of both bim^- and $2M56Dfbim^-$ ligands along with Cd(II). (g) First 4 membered ring is represented by green rectangle and it is formed by both bim^- and $2M56DFbim^-$ ligands along with Cd(II). (h) Second 4 membered ring is represented by magenta rectangle and it formed by only bim ligands along with Cd(II). Grey, dark blue, beige, and green spheres represent C, N, Cd, and F atoms, respectively; hydrogen atoms are omitted for clarity.

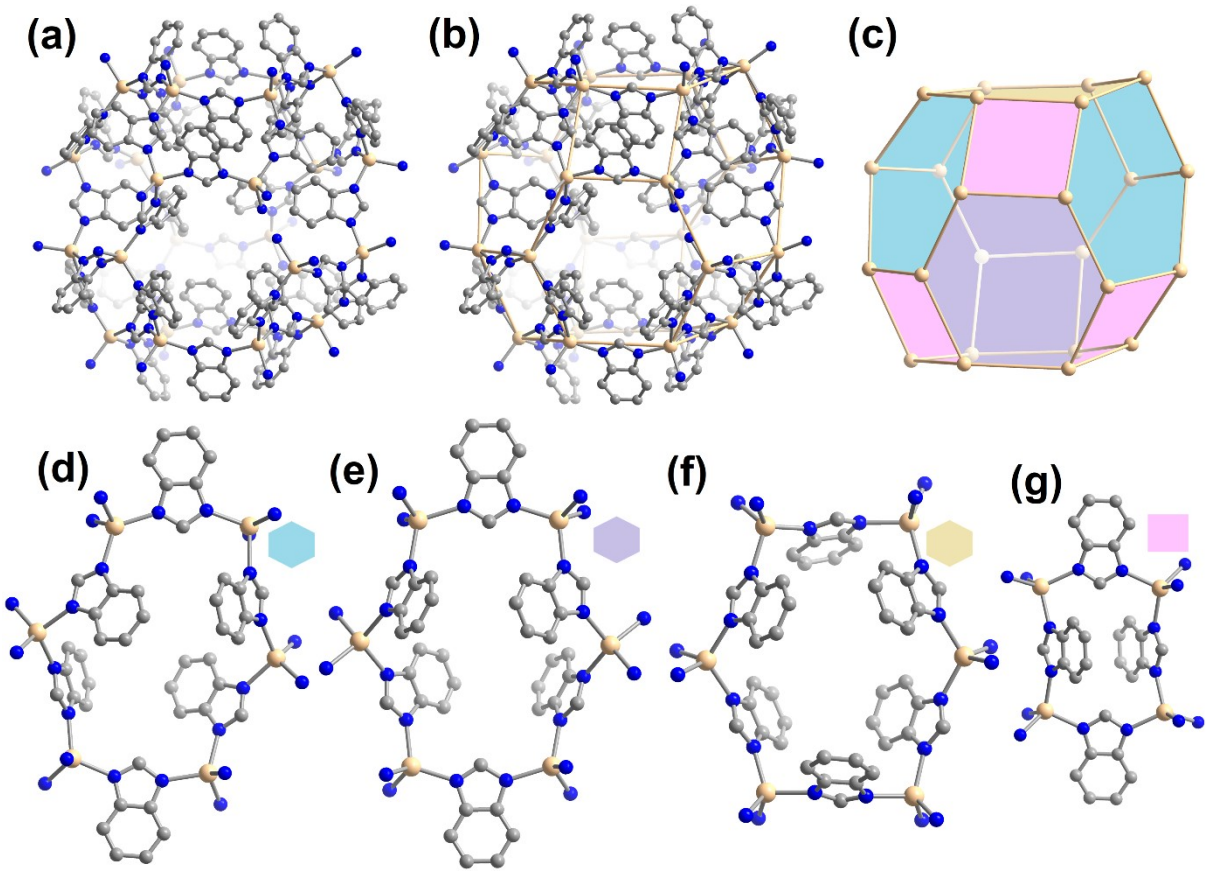

Fig. S40. Portions of the previously published *N,N*-dimethylformamide-solvated structure for CdIF-13 in the $P2_1/n$ space group, are shown here (adapted from reference 2). (a) Individual sodalite cage found in the *N,N*-dimethylformamide-solvated CdIF-13, is constructed by the Cd(II) and bim ligands. (b) Individual cage with the underlying skeleton of the structure present in the *N,N*-dimethylformamide-solvated CdIF-13. (c) Sodalite-like topology is formed by the constituent skeleton of 4 and 6 membered rings comprised by Cd(II) and bim^- ligands. Different rings in the structure can be identified by the colored polygons. (d) The blue hexagon represents the first 6 membered ring. (e) The second 6 membered ring is represented by the purple hexagon. (f) The third 6 membered ring is represented by yellow hexagon. (g) The 4 membered rings are represented by the pink rectangle. Grey, dark blue and beige, spheres represent C, N, and Cd, respectively; hydrogen atoms are omitted for clarity.

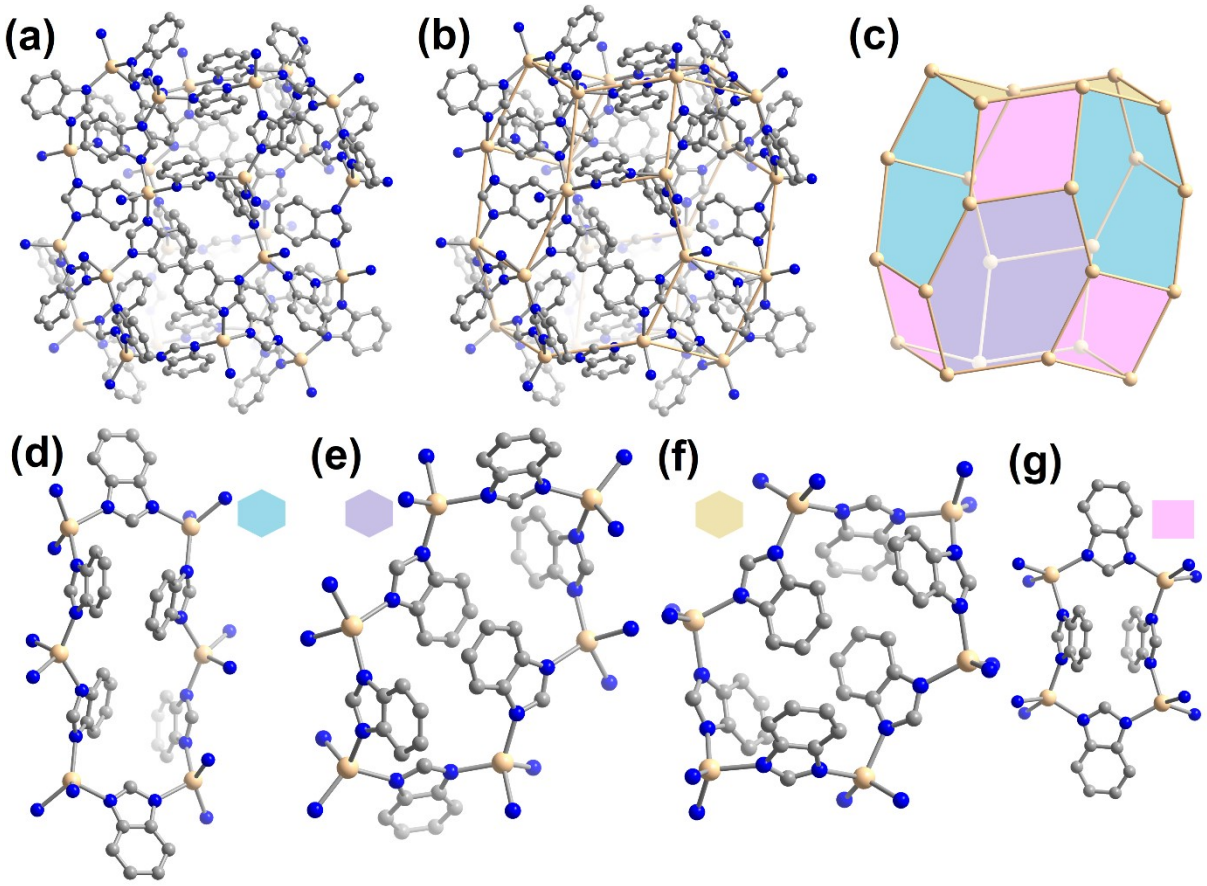

Fig. S41. Portions of the previously published structure for activated CdIF-13 in the *P*ī space group, are shown here (adapted from reference 8). (a) Individual sodalite cage found in the activated CdIF-13 structure, is constructed by the Cd(II) and bim⁻ ligands. (b) Individual cage with the underlying skeleton of the structure present in the activated CdIF-13. (c) Sodalite-like topology is formed by the constituent skeleton of 4 and 6 membered rings comprised by Cd(II) and bim⁻ ligands. Different rings in the structure can be identified by the colored polygons. (d) The blue hexagon represents the first 6 membered ring. (e) The second 6 membered ring is represented by the purple hexagon. (f) The third 6 membered ring is represented by the yellow hexagon. (g) The 4 membered rings are represented by the pink rectangle. Grey, dark blue and beige, spheres represent C, N, and Cd, respectively; hydrogen atoms are omitted for clarity.

Summary of Pawley Fitting

Pawley fits were performed using TOPAS Academic.[9] Lattice parameters were extracted from the Pawley fits of these patterns (Tables S2, S3). The activated materials crystallize in either the the $P\bar{1}$ or the $P2_1/n$ space groups, with lattice parameters that are very similar to the known compounds in the sodalite-like topology.[2,8,10] The re-solvated materials crystallize in the $P2_1/n$ space group with lattice parameters similar to those for CH_2Cl_2-solvated CdIF-13.[2] Therefore, we hypothesize that these compounds assume and do not deviate from the sodalite-like topology with the exception of the 5:4 compound, which displays unique triclinic parameters in the activated phase. We find a minor cadmium carbonate[11] impurity in some of the compounds. We find a small amount of the $P\bar{1}$ structure as a minor phase in the 7:1 species.

Table S2. Lattice parameters for activated or partially activated materials. Here S.G. stands for space group and GoF stands for Goodness of Fit. Errors in parentheses represent ±1σ. Materials are listed based on the synthetic ratio of the benzimidazole:2-methyl-5,6-difluorobenzimidazole. $P2_1/n$ phase lattice parameters found for the 7:1 material are also included in the the following table.

	S.G.	*a* (Å)	*b* (Å)	*c* (Å)	α (°)	β (°)	γ (°)	V (Å^3)
5:4	$P\bar{1}$	11.233(4)	14.552(4)	16.883(8)	102.77(3)	88.07(6)	111.90(4)	2493.5(7)
	R_{wp} (%):	6.779	R_p (%):	5.316	R_{exp} (%):	4.795	GoF:	1.414
4:1	$P2_1/n$	13.976(3)	22.350(6)	16.333(7)	90	114.82(2)	90	4630.5(7)
	R_{wp} (%):	8.624	R_p (%):	6.246	R_{exp} (%):	4.454	GoF:	1.897
5:1	$P2_1/n$	13.226(5)	21.904(7)	16.443(5)	90	113.00(1)	90	4385.0(3)
	R_{wp} (%):	12.983	R_p (%):	9.892	R_{exp} (%):	8.451	GoF:	1.536
6:1	$P2_1/n$	13.592(1)	22.099(5)	16.408(3)	90	113.272(6)	90	4527.7(2)
	R_{wp} (%):	12.042	R_p (%):	8.843	R_{exp} (%):	7.934	GoF:	1.518
7:1	$P2_1/n$	13.53(3)	22.03(2)	16.24(5)	90	112.9(1)	90	4460(4)
	$P\bar{1}$	11.42(2)	14.44(2)	14.24(2)	115.3(2)	92.88(8)	105.5(2)	2011(2)
	R_{wp} (%):	6.820	R_p (%):	4.914	R_{exp} (%):	4.615	GoF:	1.478
14:1	$P\bar{1}$	11.076(3)	14.782(4)	15.036(6)	112.30(3)	92.60(2)	106.31(2)	2153.8(3)
	R_{wp} (%):	4.369	R_p (%):	3.361	R_{exp} (%):	3.186	GoF:	1.371

Table S3. Lattice parameters for resolvated materials. Here S.G. stands for space group and GoF stands for Goodness of Fit. Errors in parentheses represent ±1σ. Materials are listed based on the synthetic ratio of the benzimidazole:2-methyl-5,6-difluorobenzimidazole.

	S.G.	*a* (Å)	*b* (Å)	*c* (Å)	α (°)	β (°)	γ (°)	V (Å^3)
5:4	$P2_1/n$	16.308(3)	23.727(5)	16.173(4)	90	112.173(3)	90	5772(2)
	R_{wp} (%):	7.070	R_p (%):	5.254	R_{exp} (%):	5.538	GoF:	1.277
4:1	$P2_1/n$	16.43(1)	24.52(1)	15.718(5)	90	111.92(3)	90	5876(6)
	R_{wp} (%):	7.873	R_p (%):	5.820	R_{exp} (%):	5.431	GoF:	1.450
5:1	$P2_1/n$	16.27(1)	23.694(8)	16.189(6)	90	112.58(3)	90	5763(5)
	R_{wp} (%):	5.639	R_p (%):	4.768	R_{exp} (%):	5.214	GoF:	1.236
6:1	$P2_1/n$	16.058(8)	23.771(5)	16.176(3)	90	112.50(3)	90	5704(1)
	R_{wp} (%):	6.308	R_p (%):	4.796	R_{exp} (%):	4.531	GoF:	1.392
7:1	$P2_1/n$	15.94(1)	23.44(4)	16.226(7)	90	113.24(6)	90	5573(2)
	R_{wp} (%):	6.420	R_p (%):	4.766	R_{exp} (%):	4.923	GoF:	1.304
14:1	$P2_1/n$	16.159(3)	23.48(1)	16.345(3)	90	112.95(2)	90	5709(1)
	R_{wp} (%):	5.781	R_p (%):	4.211	R_{exp} (%):	4.575	GoF:	1.264

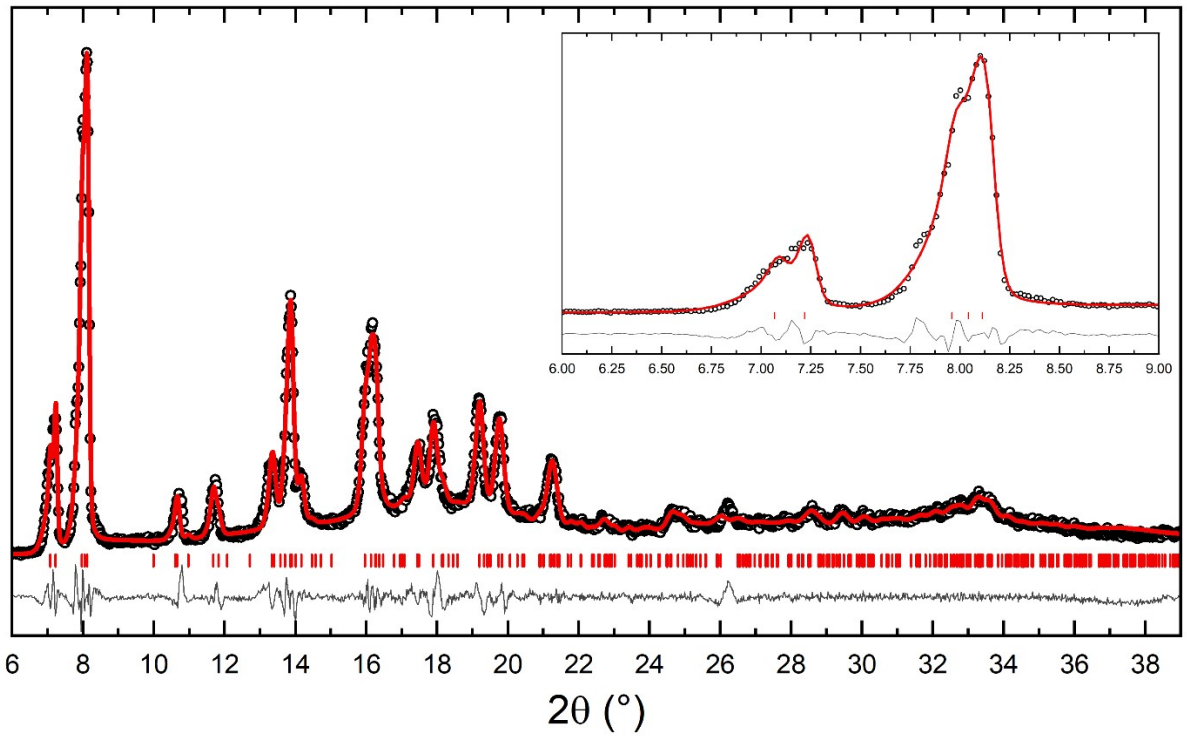

Fig. S42. Pawley fit of the activated 4:1 benzimidazole:2-methyl-5,6-difluorobenzimidazole species. The open black circles, red line, gray line, and vertical tick marks represent the data, the Pawley fit, the difference curve, and the *hkl* positions, respectively. Error bars are smaller than or commensurate with symbols and represent ±1σ. λ = 1.5406 Å.

Fig. S43. Pawley fit of the activated 5:1 benzimidazole:2-methyl-5,6-difluorobenzimidazole species. The open black circles, red line, gray line, and vertical tick marks represent the data, the Pawley fit, the difference curve, and the *hkl* positions, respectively. Error bars are smaller than or commensurate with symbols and represent ±1σ. λ = 1.5406 Å.

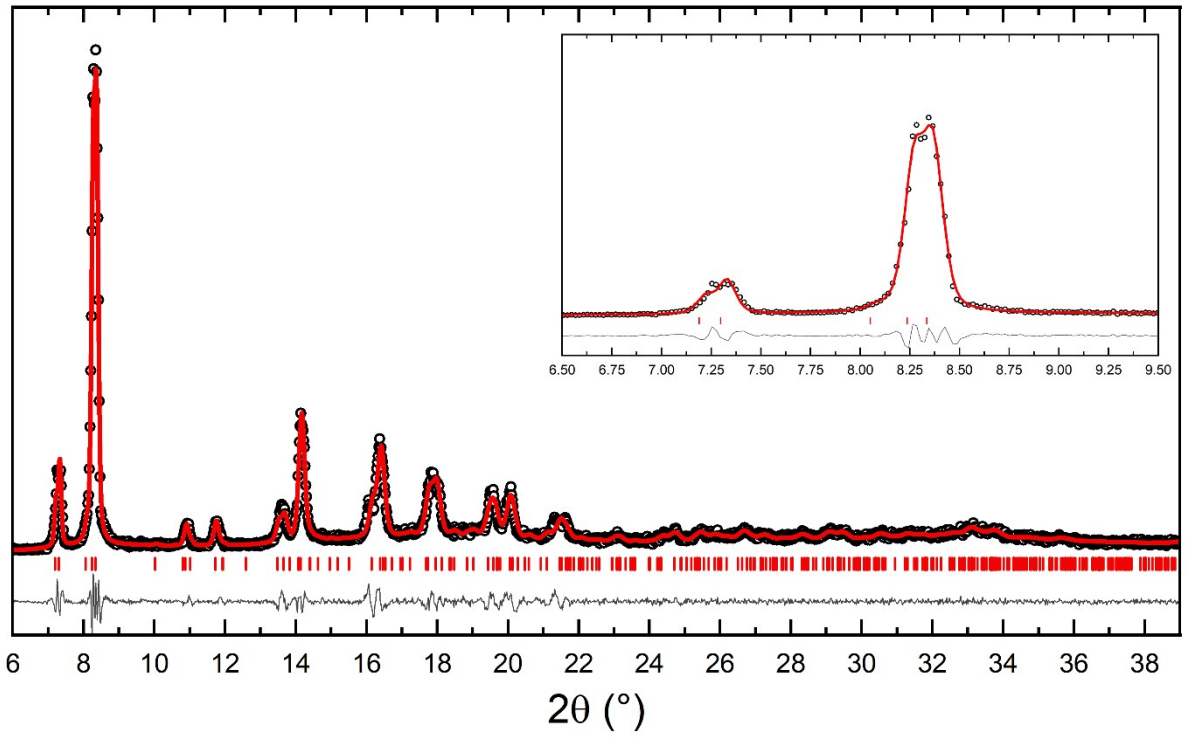

Fig. S44. Pawley fit of the activated 6:1 benzimidazole:2-methyl-5,6-difluorobenzimidazole species. The open black circles, red line, gray line, and vertical tick marks represent the data, the Pawley fit, the difference curve, and the *hkl* positions, respectively. Error bars are smaller than or commensurate with symbols and represent ±1σ. λ = 1.5406 Å.

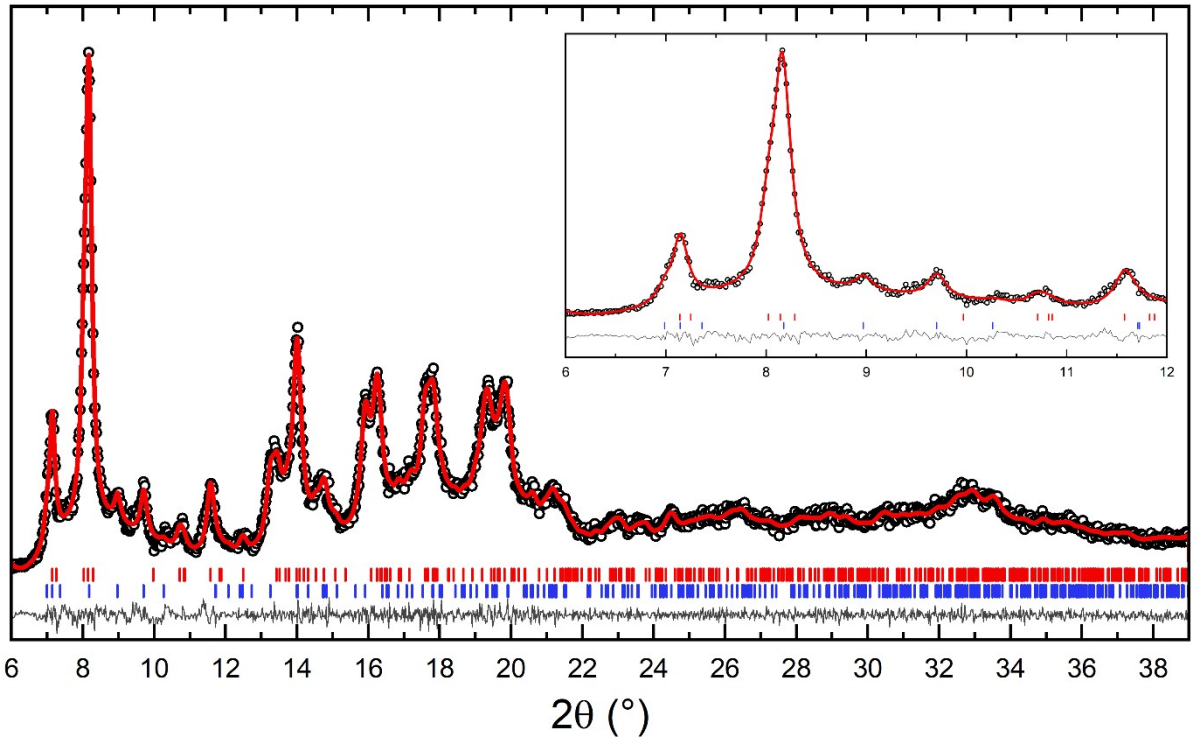

Fig. S45. Pawley fit of the activated 7:1 benzimidazole:2-methyl-5,6-difluorobenzimidazole species. The open black circles, red line, gray line, and red and blue vertical tick marks represent the data, the Pawley fit, the difference curve, and the *hkl* positions for the $P2_1/n$ and $P\bar{1}$ phases, respectively. Error bars are smaller than or commensurate with symbols and represent ±1σ. λ = 1.5406 Å.

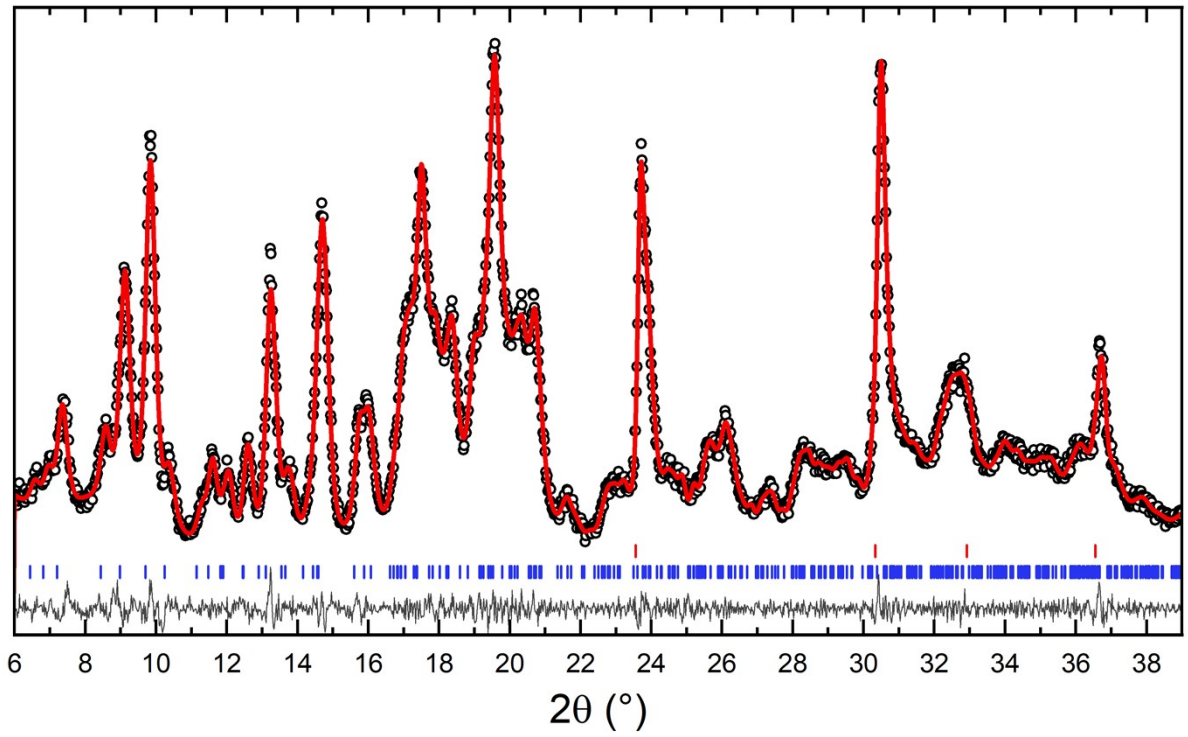

Fig. S46. Pawley fit of the activated 14:1 benzimidazole:2-methyl-5,6-difluorobenzimidazole species. The open black circles, red line, gray line, and blue and red vertical tick marks represent the data, the Pawley fit, the difference curve, and the *hkl* positions for the $P2_1/n$ and $CdCO_3$ impurity phases, respectively. Error bars are smaller than or commensurate with symbols and represent ±1σ. λ = 1.5406 Å.

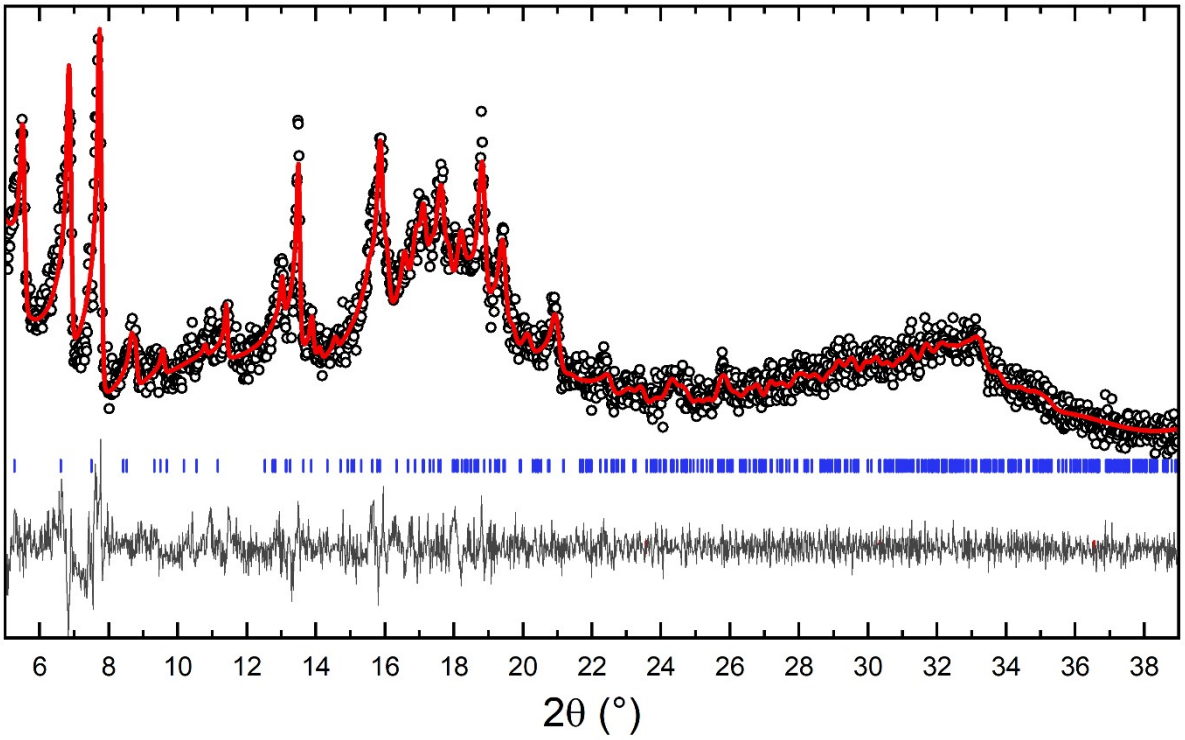

Fig. S47. Pawley fit of the activated 5:4 benzimidazole:2-methyl-5,6-difluorobenzimidazole species. The open black circles, red line, gray line, and red and blue vertical tick marks represent the data, the Pawley fit, the difference curve, and the *hkl* positions, respectively. Error bars are smaller than or commensurate with symbols and represent ±1σ. λ = 1.5406 Å.

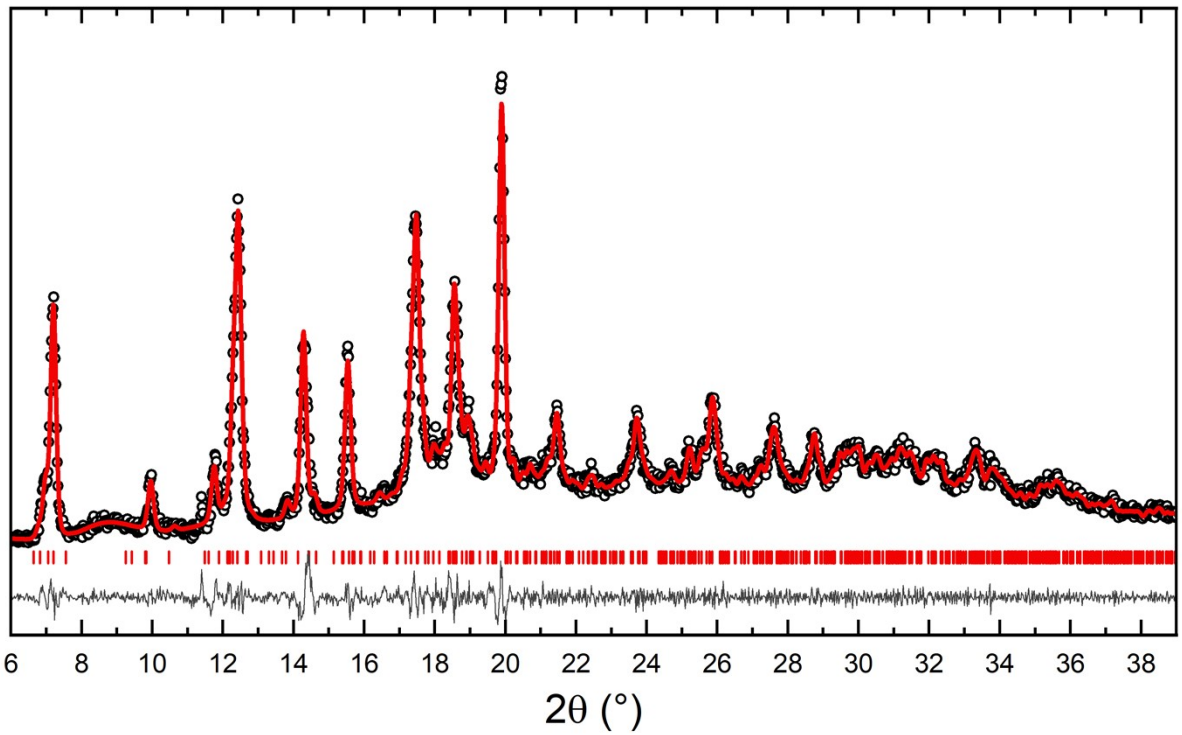

Fig. S48. Pawley fit of the resolvated 4:1 benzimidazole:2-methyl-5,6-difluorobenzimidazole species. The open black circles, red line, gray line, and red and blue vertical tick marks represent the data, the Pawley fit, the difference curve, and the *hkl* positions, respectively. Error bars are smaller than or commensurate with symbols and represent ±1σ. λ = 1.5406 Å.

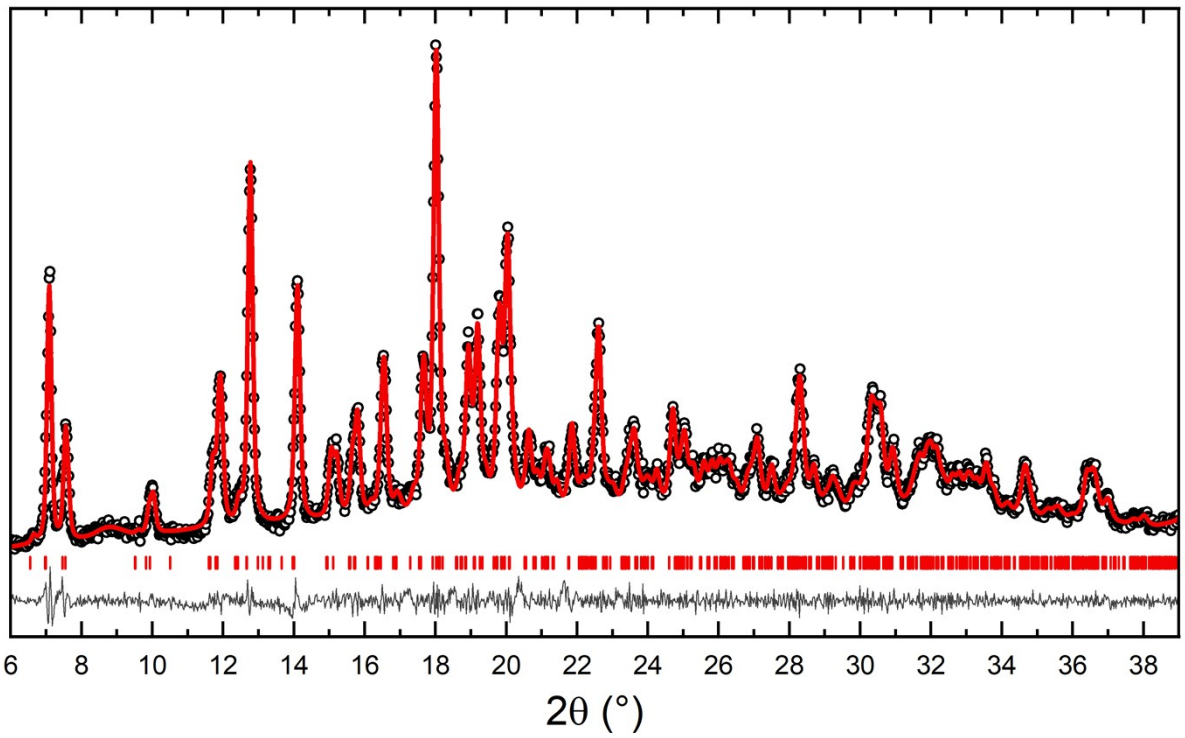

Fig. S49. Pawley fit of the resolvated 5:1 benzimidazole:2-methyl-5,6-difluorobenzimidazole species. The open black circles, red line, gray line, and red and blue vertical tick marks represent the data, the Pawley fit, the difference curve, and the *hkl* positions, respectively. Error bars are smaller than or commensurate with symbols and represent ±1σ. λ = 1.5406 Å.

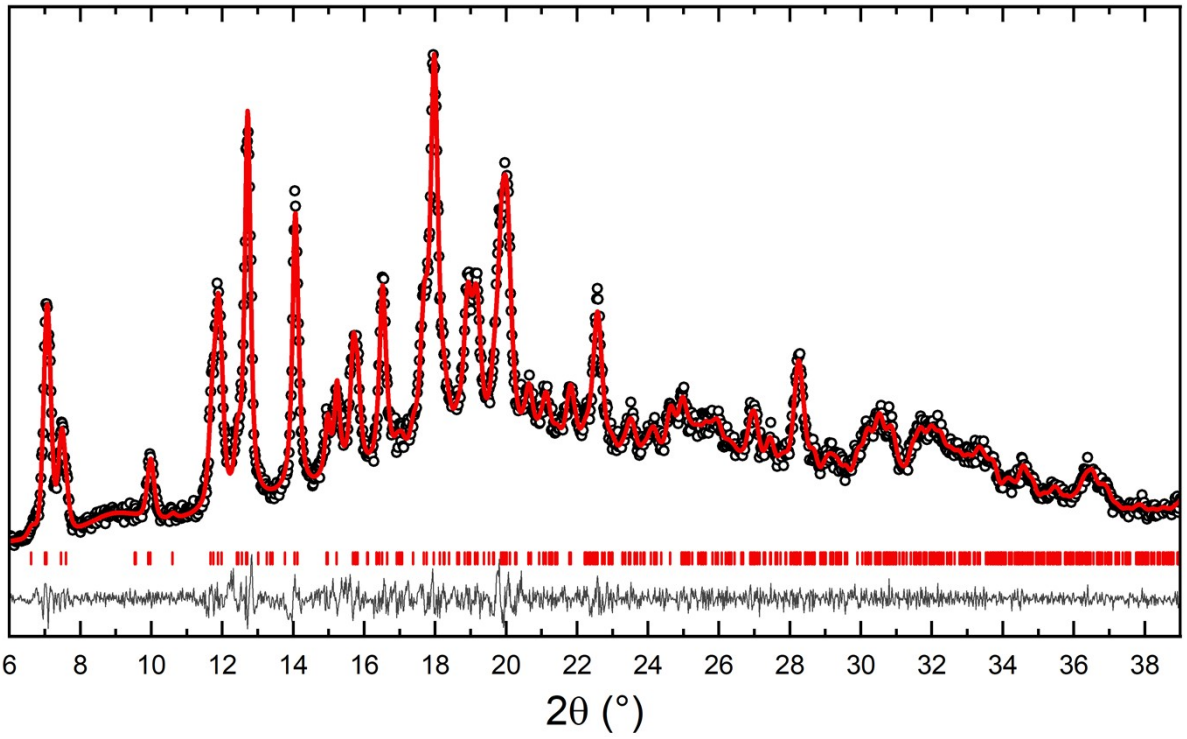

Fig. S50. Pawley fit of the resolvated 6:1 benzimidazole:2-methyl-5,6-difluorobenzimidazole species. The open black circles, red line, gray line, and red and blue vertical tick marks represent the data, the Pawley fit, the difference curve, and the *hkl* positions, respectively. Error bars are smaller than or commensurate with symbols and represent ±1σ. λ = 1.5406 Å.

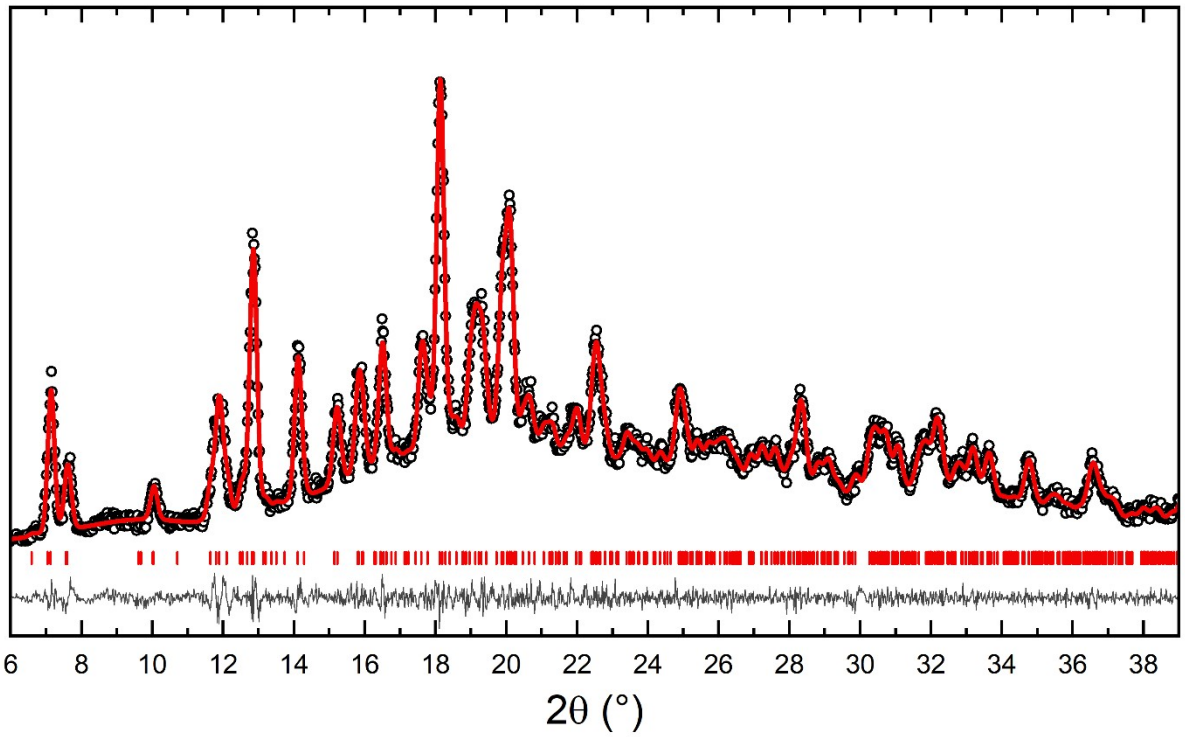

Fig. S51. Pawley fit of the resolvated 7:1 benzimidazole:2-methyl-5,6-difluorobenzimidazole species. The open black circles, red line, gray line, and red and blue vertical tick marks represent the data, the Pawley fit, the difference curve, and the *hkl* positions, respectively. Error bars are smaller than or commensurate with symbols and represent ±1σ. λ = 1.5406 Å.

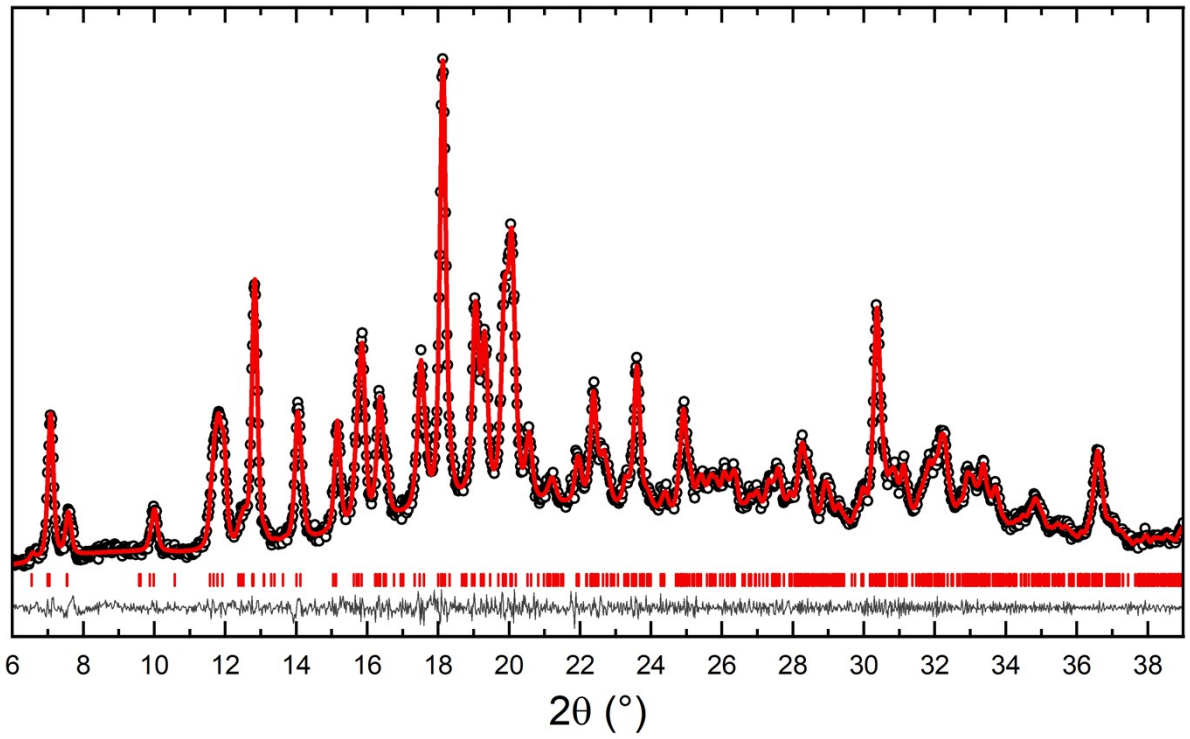

Fig. S52. Pawley fit of the resolvated 14:1 benzimidazole:2-methyl-5,6-difluorobenzimidazole species. The open black circles, red line, gray line, and red and blue vertical tick marks represent the data, the Pawley fit, the difference curve, and the *hkl* positions, respectively. Error bars are smaller than or commensurate with symbols and represent ±1σ. λ = 1.5406 Å.

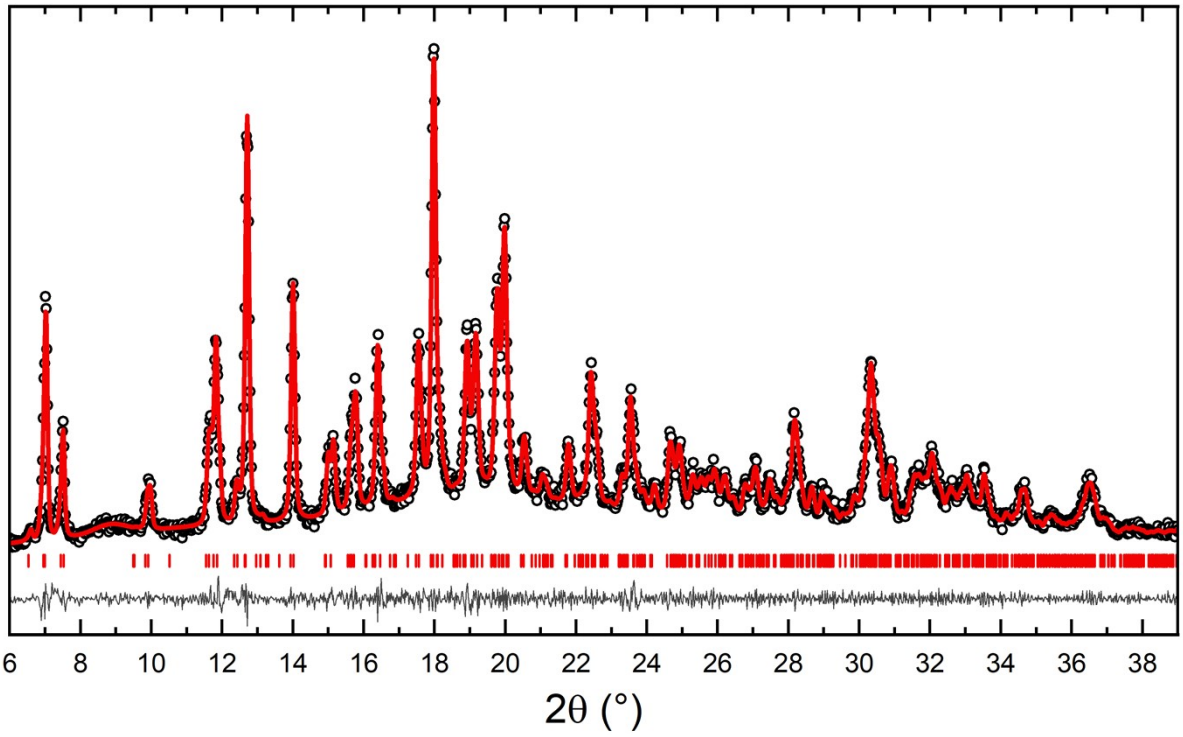

Fig. S53. Pawley fit of the resolvated 5:4 benzimidazole:2-methyl-5,6-difluorobenzimidazole species. The open black circles, red line, gray line, and red and blue vertical tick marks represent the data, the Pawley fit, the difference curve, and the *hkl* positions, respectively. Error bars are smaller than or commensurate with symbols and represent ±1σ. λ = 1.5406 Å.

References

1. B. Kriete, A. S. Bondarenko, V. R. Jumde, L. E. Franken, A. J. Minnaard, T. L. C. Jansen, J. Knoester and M. S. Pshenichnikov, *J. Phys. Chem. Lett*., 2017, **8**, 2895–2901.

2. C. M. McGuirk, T. Runčevski, J. Oktawiec, A. Turkiewicz, M. K. Taylor and J. R. Long, *J. Am. Chem. Soc.*, 2018, **140**, 15924–15933.

3. O. V. Dolomanov, L. J. Bourhis, R. J. Gildea, J. A. K. Howard and H. Puschmann, *J. Appl. Cryst*. 2009, **42**, 339–341.

4. G. M. Sheldrick, *Acta Cryst. A*, 2015, **71**, 3–8.

5. G. M. Sheldrick, *Acta Cryst. A*, 2008, **64**, 112–122.

6. A. Thorn, B. Dittrich and G. M. Sheldrick, *Acta Cryst. A*, 2012, **68**, 448–451.

7. C. F. Macrae, P. R. Edgington, P. McCabe, E. Pidcock, G. P. Shields, R. Taylor, M. Towler, J. van de Streek, J. Appl. Cryst. 2006, 39, 453– 457.

8. R. A. Klein, S. Shulda, P. A. Parilla, P. Le Magueres, R. K. Richardson, W. Morris, C. M. Brown and C. M. McGuirk, *Chem. Sci.*, 2021, **12**, 15620–15631.

9. A. Coelho, Topas Academic v6; Coelho Softw. (2017). http://www.topas-academic.net/.

10. K. S. Park, Z. Ni, A. P. Côté, J. Y. Choi, R. Huang, F. J. Uribe-Romo, H. E. Chae, M. O'Keefe and O. M. Yaghi, *Proc. Natl. Acad. Sci. U. S. A*., 2006, **103**, 10186–10191.

11. V. Borodin, V. Lyutin, V. Ilyukhin and N. Belov, *Doklady Akademii Nauk SSSR*, 1979, **245**, 1099–1101.